

1    **Conservation of EMT transcription factor function in controlling pluripotent**  
2    **adult stem cell migration *in vivo* in planarians**

3

4    Prasad Abnave<sup>1</sup>, Ellen Aboukhatwa<sup>1</sup>, Nobuyoshi Kosaka<sup>1</sup>, James Thompson<sup>2</sup>, Mark A.  
5    Hill<sup>2</sup>, A. Aziz Aboobaker<sup>1\*</sup>

6

7    1. Department of Zoology, Tinbergen Building, South Parks Road, University of  
8    Oxford, Oxford OX1 3PS, United Kingdom

9    2. CRUK/MRC Oxford Institute for Radiation Oncology, ORCRB Roosevelt Drive,  
10    University of Oxford, Oxford OX3 7DQ, United Kingdom

11

12    \*Correspondence: [Aziz.Aboobaker@zoo.ox.ac.uk](mailto:Aziz.Aboobaker@zoo.ox.ac.uk)

13

14    Lead Contact

15    [Aziz.Aboobaker@zoo.ox.ac.uk](mailto:Aziz.Aboobaker@zoo.ox.ac.uk)

16

17

18 **SUMMARY**

19

20 Migration of stem cells underpins the physiology of metazoan animals. For tissues to be  
21 maintained, stem cells and their progeny must migrate and differentiate in the correct  
22 positions. This need is even more acute after tissue damage by wounding or pathogenic  
23 infections. Inappropriate migration also underpins the formation of metastasis. Despite  
24 this, few mechanistic studies address stem cell migration during repair or homeostasis  
25 in adult tissues. Here, we present a shielded X-ray irradiation assay that allows us to  
26 follow stem cell migration in the planarians. We demonstrate that we can use this  
27 system to study the molecular control of stem cell migration and show that *snail* and  
28 *zeb-1* EMT transcription factors homologs are necessary for cell migration to wound  
29 sites and for the establishment of migratory cell morphology. Our work establishes  
30 planarians as a suitable model for further in depth study of the processes controlling  
31 stem cell migration in vivo.

32

33 **Keywords: stem cells, planarian, regeneration, migration, *snail*, *zeb-1*, EMT,**  
34 **wounding, *notum*, differentiation.**

35

## 36 INTRODUCTION

37 Regeneration and tissue homeostasis in multicellular animals are a result of the activity  
38 of their stem cells. Most animal adult life histories include some potential to regenerate  
39 lost cells, tissues and organs but the efficiency and extent of the regenerative process  
40 varies greatly amongst species. Many basal invertebrates like cnidarians, flatworms and  
41 annelids are capable of whole body regeneration and some of these are now  
42 experimentally tractable model organisms for studying regeneration and homeostasis  
43 (Galliot, 2012; Gehrke and Srivastava, 2016; Tanaka and Reddien, 2011). Studies of the  
44 invertebrate stem cells that contribute to regeneration and homeostasis inform us about  
45 the origins of key stem cell properties. These include potency, self-renewal, production  
46 of the correct quantity and type of progeny, and the interpretation of positional  
47 information to ensure regenerated tissue is patterned and functionally integrated. So far  
48 few studies in regenerative models have investigated cell migration *in vivo* in adult  
49 animals, even though migration to sites of injury or homeostatic activity is a key stem  
50 cell activity for regeneration and repair, and has important biomedical applications  
51 (Bradshaw et al., 2015; Guedelhofer and Sánchez Alvarado, 2012a; Reig et al., 2014).  
52 The over-activity of migratory mechanisms is a feature of tumor tissue invasion and the  
53 pathology caused by cancers (Friedl and Gilmour, 2009; Friedl et al., 2012). Defects in  
54 stem cell migration are likely to contribute to many age-related processes leading to  
55 disease. These links remain poorly described, particularly *in vivo* (Goichberg, 2016).  
56 Many studies have revealed common mechanisms that drive cell migration in different  
57 contexts (Friedl and Alexander, 2011; Friedl et al., 2012; Goichberg, 2016; Ridley et  
58 al., 2003). However, studying cell migration *in vivo* is technically challenging, and  
59 simple model systems amenable to functional study may have a lot to offer. For  
60 example, *in vivo* studies in both *Drosophila* and *C. elegans* during embryogenesis and  
61 larval development have proven very useful for unveiling fundamental molecular

62 mechanisms also used by vertebrates (Geisbrecht and Montell, 2002; Hagedorn et al.,  
63 2013; Montell, 2003; Reig et al., 2014; Sato et al., 2015). The planarian system, in  
64 which pluripotent adult stem cells (known as neoblasts, NBs) and their progeny can be  
65 easily identified and studied, is another potentially tractable system for studying cell  
66 migration (Eisenhoffer et al., 2008). In particular, planarians offer the potential to study  
67 stem cell migration in both an adult and highly regenerative context.

68 Here we have used the model planarian *Schmidtea mediterranea* to establish methods to  
69 study cell migration and show that NB and progeny migration utilize epithelial-  
70 mesenchymal transition (EMT) related mechanisms in response to tissue damage. To  
71 date relatively little focus has been given to stem cell migration in planarians  
72 (Guedelhofer and Sánchez Alvarado, 2012a; Saló and Baguña, 1985), although it is a  
73 necessary component of a successful regenerative outcome. We perfect an assay to  
74 allow observation of cell migration and describe several novel phenomena in the  
75 planarian system, including homeostatic cell migration mechanisms in the absence of  
76 wounding. Migrating cells form extended processes, the frequency of which correlate  
77 with cell movement towards the wound site. Using markers of the well characterized  
78 epidermal lineage we uncover a close relationship between known NB and progeny  
79 lineages and the order and extent of cell migration, demonstrating that cells at some  
80 stages of differentiation are more migratory than others. RNAi can be efficiently  
81 employed within our migration assay and we demonstrate the requirement for a  
82 planarian matrix-metalloprotease, *Smed-MMPa* (*mmpa*), and an ortholog of beta-  
83 integrin, *Smed- $\beta$ 1-integrin* ( *$\beta$ 1-integrin*), for normal cell migration and the formation of  
84 extended processes as proof of principle of this approach (Bonar and Petersen, 2017;  
85 Isolani et al., 2013; Seebeck et al., 2017). Using RNAi we also show the polarity  
86 determinant *Smed-notum* (*notum*) is necessary for homeostatic anterior migration of  
87 cells in unwounded animals, but not for cells to form processes or to migrate in

88 response to wounding (Petersen and Reddien, 2011). Our observations of migratory cell  
89 behavior and morphology led us to consider if EMT related mechanisms are likely to  
90 control cell migration in planarians. We investigated three planarian orthologs of EMT-  
91 transcription factors (EMT-TFs) and found that they were all required for stem cell  
92 migration in the context of our assay. Our work establishes the conservation of EMT  
93 mechanisms controlling cell migration across the breadth of bilaterians and establishes  
94 the use of *S. mediterranea* as a highly effective model system to study in vivo adult  
95 stem cell migration in a regenerative context.

96

## 97 **RESULTS**

### 98 **Establishment of an X-ray shielded irradiation assay for tracking stem cell** 99 **migration**

100 The sensitivity of planarian regenerative properties to high doses of ionizing radiation  
101 was established over a century ago (Bardeen and Baetjer, 1904). Later this was  
102 attributed to the fact that NBs were killed by irradiation (Wolff, 1962). Partially  
103 exposing planarians to ionizing radiation, through use of a lead shield, was shown to  
104 slow down regenerative ability and suggested the possibility that NBs were potentially  
105 able to move to exposed regions and restore regenerative ability (Dubois, 1949).  
106 Recently established methods for tracking cell migration in planarians have either  
107 revisited shielding or involved transplanting tissue with stem cells into lethally  
108 irradiated hosts (Guedelhofer and Sánchez Alvarado, 2012a; Tasaki et al., 2016).  
109 These methods clearly show movement of NBs and their progeny. We set out with the  
110 goal of adapting the shielding approach to establish a practical assay for studying the  
111 molecular control of cell migration. We wished to simultaneously use both smaller  
112 animals and larger numbers of animals for irradiation to generate a much smaller

113 shielded region and by performing experiments simultaneously across larger numbers  
114 of animals, rather than shielding animals individually.

115 We perfected a technique in which multiple animals can be uniformly irradiated with X-  
116 rays, apart from a thin strip in a predetermined position along their body axis. This is  
117 achieved by placing the animals directly above a 0.8 mm strip of lead (6.1 mm thick), to  
118 significantly attenuate the X-rays in the region just above the lead to less than 5% of the  
119 dose in the rest of the animal (Figure 1A-C, Figure S1A-C).

120 Our final working version of the apparatus is conveniently designed to fit a standard 60  
121 mm Petri dish, with the lead shield lying below the diameter (Figure 1A, Figure S1A  
122 and B). Anaesthetized planarians are aligned across the diameter in preparation for X-  
123 ray exposure (Figure 1 A-C). We could then expose up to 20 ~3-5mm long worms  
124 simultaneously to a normally lethal 30 Gy X-ray dose in a 1 min 18 sec exposure, with  
125 the shielded region receiving <1.5 Gy. This allows for some precision in controlling the  
126 position of a surviving band of NBs (Figure 1D and E).

127 Looking at animals with the shield positioned centrally along the anterior to posterior  
128 (AP) axis we performed whole mount fluorescent in situ hybridization (WFISH) to  
129 assay the effectiveness of the shield. With the *smedwi-1* NB marker we confirmed that  
130 all NBs (*smedwi-1*<sup>+</sup>) outside the shielded region disappear by 24 hours post irradiation  
131 (pi). With the early epidermal lineage marker *prog-1* we confirmed that stem cell  
132 progeny (*prog-1*<sup>+</sup>) outside the shielded region have differentiated by 4 days pi and  
133 disappear as no NB are present to renew the *prog-1*<sup>+</sup> population (Figure 1E and F). We  
134 observed that cells within the shield have a density equivalent to that in wild type  
135 animals not subjected to shielded irradiation, suggesting that the shield is effective at  
136 protecting cells (Figure 1E and F and see Figure 2D for quantification). We also noted  
137 that there is no cell migration from the shielded region during this time (Figure 1E and  
138 F). These data established that any observation of migrating NBs and progeny should

139 ideally occur after 4 days pi. In summary, our X-ray shielded assay allows convenient  
140 and precise observation of NB and progeny behavior over time post-irradiation, and in  
141 animals of a size and number suitable for functional studies.

142

### 143 **Features of planarian cell migration after wounding**

144 We next employed the assay system to describe the movement of NBs and progeny.  
145 The cycling NBs in *S. mediterranea* are normally present throughout the body but  
146 absent from the region in front of the photoreceptors and the centrally positioned  
147 pharynx and are not detectable within early regenerative blastema (Figure S2A and B).  
148 These facts mean that in normal animals: i) NBs would not normally have far to migrate  
149 during normal homeostasis or regeneration as they will always be relatively close to  
150 where they are required, except for the anterior region and the pharynx, ii) in the  
151 context of early regeneration post-mitotic progeny migrate to establish the blastema  
152 tissue before NBs, and iii) at least for the pharynx and the most anterior tissue,  
153 homeostasis is achieved by migration of post-mitotic progeny, and not NBs. Together  
154 this led us to expect that stem cell progeny might have migratory properties that are  
155 distinct from NBs.

156 We shielded animals over the pharynx (Figure 2A and B) and made anterior wounds by  
157 decapitation just under the photoreceptors, at 4 d pi when a ‘blank canvas’ is present  
158 anterior to the shielded region (Figure 1F). Using WFISH over a 10 day time course  
159 after wounding, we observed that, as previously described, stem cells and stem cell  
160 progeny migrated anteriorly towards the wound, but not in a posterior direction (Figure  
161 2B). We used the lack of posterior migration in this experimental design to facilitate  
162 accurate measurements of individual cell migration distances over time (Figure 2A).  
163 Quantifying *smedwi-1*<sup>+</sup> NBs, *prog1*<sup>+</sup> progeny and mitotic cells in the migratory region

164 just anterior to the pharynx allowed us to develop a detailed overview of the migration  
165 process (Figure 2B-E).

166 While the most advanced *smedwi-1*<sup>+</sup> cells can some times match the extent of migration  
167 of the most advanced *prog1*<sup>+</sup> cells, we found that many more *prog1*<sup>+</sup> cells enter the  
168 migratory region than *smedwi-1*<sup>+</sup> cells over the first 4 days post amputation (pa).  
169 (Figure 2B-D). This observation suggests that progeny react *en masse* to a wound  
170 derived signal and NBs follow, either independently in response to the wound signal or  
171 because they somehow sense the migration of *prog1*<sup>+</sup> cells and follow, or some  
172 combination of both. By 7 days pa, while the density of NBs and progeny in the  
173 migratory region just anterior to the shield are still lower than in unexposed animals,  
174 homeostatic ratios of stem cells and stem cell progeny are restored (Figure 2D). We  
175 observed cells in M-phase within the field of migrating cells, the numbers of which  
176 increased in proportion with the numbers of migrating *smedwi-1*<sup>+</sup> NBs over time  
177 (Figure S2C, D and Figure 2E). This pattern of proliferation in the migratory region is  
178 consistent with the homeostatic ratio of NBs and progeny being restored by increased  
179 stem cell division as well as by further migration from the shielded region (Figure 2C-  
180 E). From this we deduce that increases in number of both NBs and progeny outside of  
181 the shielded region are fueled initially by migration, but then by both further migration  
182 and proliferation of NBs.

183 *Prog1*<sup>+</sup> progeny that reach the wound site at 10 days pa can only have arisen from  
184 asymmetric cell divisions of NBs as old as 6 days pa or later, as 4 days the maximum  
185 time before they differentiate and stop expressing the *prog-1* marker (Eisenhoffer et al,  
186 2008). Given the NB migration speeds we observe (Figure 2C), these *prog1*<sup>+</sup> cells must  
187 be the progeny of NBs that have themselves already migrated well beyond the shielded  
188 region. Taken together, this data suggests that migrating *smedwi-1*<sup>+</sup> NBs undergo both  
189 symmetric and asymmetric cell divisions that increase both the number of *smedwi-1*<sup>+</sup>



190 cells and *prog1*<sup>+</sup> cells, importantly providing a source of stem cell progeny that do not  
191 derive from the shielded region. We note the overall similarity in these dynamics to that  
192 observed during regeneration after amputation, where stem cell progeny form the initial  
193 regeneration blastema, with NBs only following later.

194 We also wished to know how precise the homing of migrating cells to wounds could be.  
195 To investigate we performed single poke wounds at the midline or notches confined to  
196 one side of the animal (Figure S2E and F). We observed that even these small injuries  
197 in relatively close proximity, promoted distinct migratory responses around each wound  
198 site, indicating that migrating cells home with precision to injuries (Figure S2E and F).  
199 Despite the absence of NBs and progeny in the whole anterior tissue field migrating  
200 stem cell progeny only migrate and collect around the wound, and do not sense the  
201 absence of NBs and progeny elsewhere (Figure S2E and F). We also observed as a  
202 general feature of migration towards the wound site that dorsal *prog1*<sup>+</sup> cells appear to  
203 migrate more rapidly than ventral cells to the same wound (Figure S2G and H), and that  
204 dorsal *smedwi-1*<sup>+</sup> cells migrate centrally while ventral stem cells migrate across the  
205 width of animals (Figure S2I).

206

### 207 **Migrating planarian cells have a distinct morphology of extended cell processes**

208 We next investigated the migrating cells themselves in more detail, to see if we could  
209 understand more about how they move in *S. mediterranea*. We imaged migrating cells  
210 after wounding and compared them to cells remaining in the shielded region that were  
211 static. We observed a significantly higher frequency of individual NBs and progeny  
212 with extended cell processes in migratory regions of injured animals than in animals  
213 that were uninjured or for cells in the shielded region that were not actively migrating  
214 (Figure 2F-I, see Figure S2J and K for different cell morphology). We did not observe  
215 any connection or alignment between cells with extended processes, and individual

216 cells migrate independently with rather than any mechanism involving collective cell  
217 movement requiring cell-cell junction contact (Friedl and Alexander, 2011; Friedl et al.,  
218 2012). This observation suggests that cell migration may involve cellular mechanisms  
219 similar to those used during classical EMT (Kalluri and Weinberg, 2009; Lamouille et  
220 al., 2014). While net movement of cells is towards the wound site, we note that cell  
221 processes can extend in all directions, not just towards the wound (Figure 2J-M). Taken  
222 together these data indicate that NBs and progeny respond to wounds with directional  
223 precision and by extending cell processes.

224

### 225 **The order and extent of cell migration recapitulates cell lineage**

226 Details of planarian NB and progeny lineages, in particular the epidermal lineage allows  
227 detailed tracking of differentiation fates (Eisenhoffer et al., 2008; Tu et al., 2015; van  
228 Wolfswinkel et al., 2014). Thus, we can use the cell type markers from these studies to  
229 label different populations of NBs and progeny (Figure 3A). We investigated the  
230 expression of these markers in migrating cells using a series of overlapping double  
231 WFIISH experiments. These allowed us to measure the extent of migration of each of  
232 these cell types and to observe the relationship between migration and differentiation  
233 (Figure 3B-M). We observed that migration distance increases for cells expressing later  
234 markers of the epidermal lineage, in particular we see a significant difference in extent  
235 of migration between *smedwi-I*<sup>+ve</sup> zeta<sup>+ve</sup> NBs and *smedwi-I*<sup>-ve</sup> zeta<sup>+ve</sup> progeny (Figure  
236 3H, I and L). These data suggest that very early post-mitotic progeny may have the  
237 highest migratory potential in the epidermal cell lineage. Again, we note that this  
238 pattern of differentiation and migration recapitulates early regeneration, where cycling  
239 NBs do not enter the blastema, which is first populated by post-mitotic progeny.

240

241 **A matrix metalloprotease and beta-integrin are both required for cell migration to**  
242 **wound sites.**

243 Having provided a detailed description of cell migration in *S. mediterranea* we next  
244 wished to test if we could study gene function in the context of migration. For this we  
245 considered candidate genes that might be required for cell migration based on both  
246 previous work in planarians and by analogy with other studies of cell migration. This  
247 led us to select *mmpa* and *β1-integrin* as strong candidates for proof of principle  
248 experiments.

249 Previous research had attempted to implicate *mmpa*, one of four matrix metalloprotease  
250 enzymes identifiable in the *S. mediterranea* genome, as having a possible role in cell  
251 migration (Isolani et al., 2013). We decided to look at the function of this gene in the  
252 context of our migration assay. We first performed RNAi in the context of normal  
253 regeneration and amputation, and observed that *mmpa(RNAi)* animals showed  
254 regeneration defects as previously described, with failure to correctly regenerate  
255 anterior or posterior tissues (Figure S3A). We then performed RNAi and amputation in  
256 the context of our assay and observed that anterior tissues regressed and that animals  
257 failed to regenerate (Figure S3B). We used WFISH to monitor the movement of  
258 *smedwi-1*<sup>+</sup> NBs and *progl-1*<sup>+</sup> stem cell progeny after *mmpa(RNAi)*, and observed almost  
259 no migration of cells compared to control *gfp(RNAi)* worms (Figure 4A, D and M, see  
260 also Figure S3M and N). Additionally, we examined the morphology of NBs and  
261 progeny and observed reduced numbers of cells with extended processes compared to  
262 migrating cells in the *gfp(RNAi)* control animals (Figure 4 B, C, E, F and N). These  
263 results confirm that this matrix metalloprotease enzyme is required to facilitate cell  
264 migration in planarians and demonstrates the potential utility of our assay in generating  
265 insights into how stem cell migration is controlled. We found that *mmpa* is only  
266 expressed at relatively low levels in stem cells and stem cell progeny, with the bulk of

267 its expression in differentiated radiation insensitive cells (Figure S3C-E) (Kao et al.,  
268 2017). We also did not detect *mmpa* expression in migrating cells (Figure S3F and G),  
269 suggesting it is instead produced by differentiated cells and required in the extracellular  
270 matrix to allow cell extensions to form and allow migration.

271 We next investigated whether  $\beta 1$ -*integrin* also had a conserved role in allowing cell  
272 migration in our assay. Integrins have conserved roles in orchestrating cell migration,  
273 providing a connection between physical actions of the actin cytoskeleton and signaling  
274 mechanisms instructing migratory activity (Mogilner and Keren, 2009; Vicente-  
275 Manzanares et al., 2009). A consideration of the recently published regenerative  
276 phenotypes for planarian  $\beta 1$ -*integrin* suggested to us that the cellular disorganization  
277 observed in these studies could be in part due to failures in migratory activity (Bonar  
278 and Petersen, 2017; Seebeck et al., 2017). We observed that  $\beta 1$ -*integrin* transcript was  
279 expressed in nearly all *smedwi-1*<sup>+</sup> NBs and about a third of migrating progeny in the  
280 migration region of wildtype animals in our assay (Figure S3H-L). We performed ( $\beta 1$ -  
281 *integrin*)*RNAi* and found that cell migration was greatly impaired compared to  
282 *gfp*(*RNAi*) controls (Figure 4G-N, Figure S3M and N). Cell process formation in NBs  
283 and progeny was also disrupted (Figure 4K, L and N). These data confirm a conserved  
284 role for  $\beta 1$ -*integrin* in NB and progeny cell migration in planarians, and along with the  
285 *mmpa*(*RNAi*) phenotype confirm that our assay can be combined with RNAi based loss  
286 of function studies.

287

### 288 **Anterior migration of stem cells and stem cell progeny in the absence of wounding**

289 While wounding will trigger migration, and in fact precise homing of NBs and progeny  
290 (Figure S2 E and F), we wished to observe what happened in the absence of wounding.  
291 We shielded animals of equal size at different positions along the AP axis and irradiated  
292 them (Figure 5A). When the shield was placed in the posterior region of worms we

293 observed tissue death and regression from the anterior towards the shield (Figure 5B).  
294 Subsequently, we observed blastema formation and normal regeneration that took up to  
295 50 d pi (Figure 5C). Using WFISH we were able to observe that NBs and progeny did  
296 not migrate until the regressing anterior tissue boundary was relatively close to the  
297 anterior of the shielded region (Figure 5D). When animals were shielded in mid body  
298 regions with the top of the shield level with the most anterior region of the pharynx we  
299 observed regression of the anterior and posterior tissue (Figure 5E). We subsequently  
300 observed blastema formation and regeneration that took up to 45 d pi (Figure 5F).  
301 WFISH revealed that in these animals NBs and progeny migrate towards the anterior  
302 (Figure 5G) and later towards the posterior once regressing tissue is close to the  
303 shielded regions. These data suggested that remaining NBs maintain local tissue  
304 homeostasis, and remain stationary within the shielded region until regressing tissue  
305 boundaries are close enough to trigger migration.

306 In contrast, for animals where the posterior of the shield was positioned level with the  
307 anterior of the pharynx we observed that worms often displayed posterior regression but  
308 not anterior regression (Figure 5H and I). The heads of these animals never regressed  
309 while tails regressed and then regenerated over several weeks (Figure 5I). WFISH  
310 subsequently revealed that NBs and progeny could migrate towards the anterior in the  
311 absence of wounding or loss of tissue homeostasis (Figure 5J). These results suggest  
312 that leaving a stripe of more anteriorly positioned cells is somehow sufficient to trigger  
313 anterior migration and maintain anterior tissue homeostasis.

314 To investigate this phenomenon further we irradiated animals with shields positioned at  
315 different points along the AP axis and performed WFISH to observe NBs and stem cell  
316 progeny migration at different time points. We were able to observe migration of cells  
317 towards the anterior in the absence of wounding as long the shield was within a set  
318 distance of the anterior tip (up to 1.2 mm in animals 3 mm in length, Figure 5K and L).

319 These data add to previous work that described that migration only occurs after  
320 wounding or when tissue homeostasis fails and tissue regression reaches remaining  
321 stem cells (Guedelhofer and Sánchez Alvarado, 2012a). We find that when stem cells  
322 and stem cell progeny in the pre-pharyngeal anterior region can migrate to the anterior  
323 in the absence of wounding and before tissue homeostasis fails. This migratory activity  
324 restores the normal anterior distribution of both NBs and progeny, suggesting the  
325 presence of anterior signals that can call NBs and progeny into the brain and anterior  
326 structures over a restricted range. These observations suggest that an anterior signal  
327 exists for encouraging cell migration in intact animals that acts at least over the brain  
328 region (Figure 5L).

329

330 ***Notum* is required for anterior cell migration in intact animals, but not after**  
331 **wounding**

332 By analogy with other systems there are clearly a large number of conserved candidate  
333 signaling pathways that could be involved in promoting cell migration. We chose to  
334 study two candidate molecules, *Smed-wnt1* (*wnt1*) and *notum* that are both upregulated  
335 at anterior wounds in planarians (Petersen and Reddien, 2009). In addition, *notum* is  
336 also expressed at the anterior medial tip of intact animals (Petersen and Reddien, 2011)  
337 and is therefore also a candidate for controlling anterior migration in the absence of  
338 wounding.

339 It has been previously shown that wounding at any sites results in the transcriptional  
340 expression of *wnt1* in muscle cells at the wound site (Witchley et al., 2013). Given that  
341 Wnt signaling has a role in regulating cell migration elsewhere (Mayor and Theveneau,  
342 2014), Wnt1 resulting from wound-induced expression could be required for cell  
343 migration to the wound in planarians. We performed *wnt1(RNAi)* and observed full  
344 penetrance of the tailless phenotype previously described for these animals (Figure

345 S4A) (Petersen and Reddien, 2009). After shielded irradiation we also observed  
346 *wnt1(RNAi)* animals were able to regenerate anterior structures completely (Figure  
347 S4B). Using WFISH we observed no effects on either NB or progeny migration after  
348 wounding, and both cell populations formed cell extensions to a similar extent to  
349 control *gfp(RNAi)* animals suggesting that *wnt1(RNAi)* has no essential role in the  
350 migration process (Figure 6A-C and G-K).

351 *Smed-notum* is also expressed in muscle cells on wounding, but only at anterior facing  
352 wounds where it is required to ensure the proper specification of anterior fates, probably  
353 by repressing Wnt signaling (Petersen and Reddien, 2011). Additionally it has a  
354 homeostatic expression pattern at the anterior margin and has previously been shown to  
355 promote the homeostasis and correct size of the brain in combination with the activity  
356 of a *wnt11-6* gene expressed in posterior brain regions (Hill and Petersen, 2015). On  
357 this basis *notum* represents a candidate molecule for both wound-induced migration and  
358 migration of cells towards anterior regions in uninjured animals. We performed  
359 *notum(RNAi)* and observed full penetrance of the double tailed phenotype previously  
360 described for these animals in a standard regeneration assay (Figure S4A) (Petersen and  
361 Reddien, 2011). After shielded irradiation and wounding we observed that while  
362 *notum(RNAi)* animals failed to regenerate normal anterior structures compared to  
363 controls, we observed no difference in migration of cells or migrating cell morphology  
364 compared to control *gfp(RNAi)* animals using WFISH (Figure 6A-F, J and K).  
365 However, when using an anteriorly positioned shield, which led to anterior migration of  
366 cells in control intact unwounded *gfp(RNAi)* animals, we observed a significant  
367 reduction in anterior migration after *notum(RNAi)* (Figure 6L-S, Figure S4C-E). This  
368 reduction in migration was not accompanied by a difference in the number of cells with  
369 cell extensions (Figure 6S), suggesting that *notum* may act by contributing a directional  
370 signal rather than controlling cellular migratory behavior of anteriorly positioned NBs

371 and progeny. These data suggest that *notum* is not essential for wound-induced cell  
372 migration but is required in the case of homeostatic anterior migration in intact animals  
373 that we uncovered in this work. It seems likely that an earlier description of a  
374 *notum/wnt11-6* regulatory circuit involved in homeostatic regulation of brain size may  
375 also have a broader role in the homeostatic maintenance of anterior regions that do not  
376 normally contain NBs (Hill and Petersen, 2015).

377

### 378 **Conserved EMT transcription factors regulate cell migration in planarians**

379 We next considered if we could establish a broad comparative context for the control of  
380 cell migration in planarians and migration in other systems, including mammals. Our  
381 observation that NBs and progeny appear to migrate individually using cell extensions  
382 to interact with the extracellular matrix and non-migratory neighboring differentiated  
383 cells suggested that they may use similar mechanisms to those attributed to EMT  
384 (Thiery and Sleeman, 2006). EMT in different contexts requires the activity of a  
385 restricted group of transcription factors (EMT-TFs) (Batlle et al., 2000; Cano et al.,  
386 2000; Colvin Wanshura et al., 2011; Lamouille et al., 2014). In planarians we identified  
387 2 members of the *snail* transcription factor family (*snail-1* and *snail-2*) of EMT-TFs and  
388 an ortholog of the Zinc finger E-box binding homeobox 1 (*zeb-1*) EMT-TF.

389 We decided to test whether any of these conserved EMT-TF genes were involved in cell  
390 migration in planarians. Previously a snail family transcription factor, *snail-2*, has been  
391 reported as being expressed in collagen positive muscle cells, in a small percentage of  
392 G2/M NBs before wounding and in ~35% of G2/M NBs after wounding (Scimone et  
393 al., 2014). To our knowledge no phenotype has been reported for a snail family gene in  
394 planarians and when we performed both *snail-1(RNAi)* or *snail-2(RNAi)* with a standard  
395 regenerative assay we observed no phenotypes, and all animals regenerated normally  
396 (Figure S5A).



397 When we performed *snail-1(RNAi)* or *snail-2(RNAi)* in the context of our migration  
398 assay, animals failed to regenerate after wounding suggesting a defect in cell migration  
399 (Figure S5B). Using WFISH experiments we observed a clear decrease in the extent of  
400 cell migration compared to *gfp(RNAi)* animals (Figure 7A, D, G and P, Figure S5M and  
401 N). This defect in migration of both NBs and progeny was accompanied by a decrease  
402 in the number of cells with cell extensions (Figure 7B, C, E, F, H, I and Q).

403 We found that both *snail-1* and *snail-2* were expressed in most *smcdwi-1<sup>+</sup>* NB cells in  
404 the migratory region after wounding (87% and 93% respectively) (Figure S5F and K).  
405 This expression patterns suggest that these EMT- have a cell autonomous role in  
406 controlling NB migration. Taken together our data suggest that cell autonomous  
407 migratory mechanisms are affected by *snail-1(RNAi)* and *snail-2(RNAi)* and establish  
408 that *snail* EMT-TFs in planarians have a conserved role in regulating cell migration in  
409 response to wound signals.

410 We also investigated the role of *zeb-1* and similar to our observations for *snail* genes,  
411 no defects were observed in *zeb-1(RNAi)* animals in a normal regeneration assay  
412 (Figure S6A). We found that *zeb-1(RNAi)* also led to a failure to regenerate correctly in  
413 our migration assay (Figure S6B). Subsequent WFISH experiments revealed clear  
414 defects in cell migration and cell process formation, very similar to those observed for  
415 both *snail* TFs (Figure 7J-Q, Figure S6H and I). While we could only detect *zeb-1*  
416 transcript expression in relatively few migrating *smcdwi-1<sup>+</sup>* NBs (8%, Figure S6C-F),  
417 this seems likely to be partly due to very low levels of transcript expression (Figure  
418 S6C-F) (Kao et al, 2017). Taken together, our data establish that conserved EMT-TFs  
419 are required for NB and progeny migration in planarians, establishing conservation of  
420 this regulatory circuit across bilaterians.

421

422 **DISCUSSION**

423 **An X-ray shielded assay allows precise observation of cell migration and**  
424 **application of functional genomic approaches**

425 We have established a robust and reliable method that allows the regenerative planarian  
426 model system to be used to study cell migration. During homeostasis as well as standard  
427 regeneration experiments, NBs and stem cell progeny are always close to where they  
428 are required. Nonetheless, as with all metazoans, NBs and progeny must still move into  
429 the correct functional positions in the tissues and organs. In the case of very anterior  
430 region and the pharynx of the planarian body plan, that are devoid of NB, homeostasis  
431 must be achieved by migration of stem cell progeny (Figure S2A and B). However  
432 precise monitoring of this process is difficult as the migratory distances involved are  
433 short and so confidently inferring changes in migratory behavior as oppose to changes  
434 in, say, differentiation is not possible. Our X-ray shielded assay creates a ‘blank canvas’  
435 into which migrating stem cells and stem cell progeny move and we can accurately  
436 assign relationships between migration, differentiation and proliferation of groups of  
437 these cells over time. We show that planarian NBs and progeny are capable of restoring  
438 full tissue and organ function by migrating from the small shielded region. The  
439 innovations we have made here compared to earlier approaches allow for a thinner  
440 shield, smaller worms to be irradiated and technical consistency over relatively large  
441 numbers of worms. This has allowed us to combine WFISH and RNAi approaches so  
442 that we can now use the planarian model to study migration in a regenerative context.

443

444 **A detailed description of migratory behavior in a regenerative context**

445 In this work we have revealed a number of detailed properties of cell migration in  
446 planarians that can be used to help unpick the mechanisms controlling cell migration.  
447 We have shown that migration occurs in response to wounding or damaged tissue as  
448 previously described (Guedelhofer and Sánchez Alvarado, 2012a). We also find that

449 contrary to previous work that migration can occur without wounding or failure in  
450 tissue homeostasis for anteriorly positioned stem cells and stem cell progeny. This  
451 observation tallies with the absence of NBs in anterior regions and the brain in intact  
452 animals, which suggests that a mechanism for encouraging homeostatic cell migration  
453 must exist. We also observe that migrating cells home precisely to wounds without  
454 initially recognizing other tissue regions also lack NBs and progeny. Finally, we  
455 observe that in regions containing moving cells we can see a clear increase in the  
456 number of cells with pronounced cell extensions. Migrating cells are unconnected to  
457 other migrating cells, and together these observations give an EMT like characteristic to  
458 planarians cell migration, as oppose to other mechanism involving collective cell  
459 migration. Taken together these observations establish a set of basic phenotypic criteria  
460 that can be used to the study the genetic and molecular control of cell migration.

461

#### 462 **The relationship between stem cell migration, proliferation and differentiation**

463 Stem cell migration during normal healthy tissue homeostasis must be intricately linked  
464 to cell divisions, differentiation and integration of new cells to ensure dysfunctional  
465 aged and damaged differentiated cells are successfully replaced. Studying this process  
466 *in vivo* during adult tissue homeostasis has proven to be challenging and remains  
467 limited to a few contexts. Highly regenerative animal models represent an opportunity  
468 to study these processes, which together power regeneration. Thus, perhaps the most  
469 important observations facilitated by our assay are those concerning the relationships  
470 between migration, proliferation and differentiation.

471 We observe that progeny migrate in large numbers in an initial response to wounding  
472 and that proliferating NBs accompany them in smaller numbers. In response to both  
473 wounding and homeostatic signals we observe that NBs divide asymmetrically as they  
474 migrate, and that the new progeny differentiate further while they migrate. For the well-

475 characterised epidermal lineage this creates an order of migration that recapitulates the  
476 order of differentiation. We do not see any evidence that progeny slow down their  
477 differentiation process in order to first reach wound sites and then differentiate. Instead  
478 our observations broadly recapitulate cell behaviour observed during regeneration, in  
479 which progeny migrate to form the regeneration blastema where they complete  
480 differentiation and cycling cells follow later. Our analysis detects significant differences  
481 in migration between *smedwi-1*<sup>+</sup> cells and zeta class/*smedwi-1*<sup>-</sup> cells, which we interpret  
482 as suggesting that newly minted progeny migrate ahead of cycling NBs as they do in  
483 blastema formation. NBs may migrate more slowly on average as they stop to divide, or  
484 because they require the presence of progeny at certain density before they can be  
485 healthily maintained in a repopulating tissue region, or simply perhaps because they are  
486 slower due to having smaller cell extensions. Based on these observations we note that  
487 our assay will provide an alternate method of assessing cell lineage relationships with  
488 WFISH approaches and when combined with RNAi it allows the molecular processes  
489 controlling the interplay between migration, proliferation and differentiation to be  
490 studied. For example, future experiments can test the requirement of migrating stem  
491 cells for stem cell progeny by interfering with differentiation of specific lineages or  
492 asymmetric division.

493 Related to the observation that the order of cell migration we observe recapitulates cell  
494 lineages is the question of whether all types of wound will result in the same or  
495 different combinations of migratory, proliferative and differentiation responses. While  
496 we have established that migration homes precisely to wound sites we can also now  
497 study if differentiation programs show specificity to the type of wounds depending on  
498 which cell types are damaged. Recently it was shown that production of photoreceptor  
499 precursors and cells was independent of whether eyes were present or not (LoCascio et  
500 al., 2017), suggesting that for some these organs at least differentiation programs are

501 independent of the state of the target tissue in planarians. Combining our assay with  
502 experimental paradigms that damage one or a few defined cell types will help begin to  
503 answer how demands for new cells are regulated and how stem cells and their progeny  
504 sense and adjust to these demands. Given that these are likely to be the processes that  
505 decline in human age related disease or are mis-regulated during tumour progression,  
506 new planarian experiments in this context will provide important insights.

507

508 **A role for *notum* in homeostatic migration of stem cells and stem cell progeny.**

509 The precise identification of the signals that trigger migration after wounding remains  
510 an open question. It seems more than likely that many overlapping signals cooperate to  
511 ensure migration occurs correctly and they may include signals associated primarily  
512 with occurrence of damage as well as signals from specific tissues that require specific  
513 progeny. Two genes that have already been shown to have complementary roles in  
514 controlling the polarity of planarian regeneration, *wnt1* and *notum*, are both known to be  
515 wound induced (Petersen and Reddien, 2011) and represented good candidates for  
516 potential roles in cell migration after wounding. In addition homeostatic expression of  
517 *notum* was recently shown to be involved in regulating planarian brain size in  
518 combination with *wnt11-6*, and specifically ensuring that sufficient neural precursors  
519 are produced to maintain the correct brain size (Hill and Petersen, 2015). These  
520 observations therefore also made *notum* a candidate for involvement in the homeostatic  
521 cell migration that we described in intact animals in anterior regions.

522 Using RNAi we found no role for either *wnt1* or *notum* in wound induced migration,  
523 however we found that *notum* is required for the homeostatic anterior migration. Given  
524 the homeostatic expression of *notum* transcript and the observation that cells migrate  
525 homeostatically within a certain distance from the anterior tip of the animal, we propose  
526 that a gradient of *notum* somehow provides directional cues to migrating cells. We note

527 that, the formation of cell extensions is not effected by *notum(RNAi)*, suggesting that  
528 other signals may be responsible for this aspect of migratory behaviour while *notum*  
529 activity provides a directional cue. *Notum* in planarians, mammals and flies has been  
530 implicated as a Wnt signaling inhibitor (Kakugawa et al., 2015; Traister et al., 2008;  
531 Zhang et al., 2015), so it is possible that inhibition of local homeostatic levels of Wnt  
532 signaling, specifically of anteriorly expressed planarian Wnts (*wnt11-6* and *wnt5*) may  
533 then allow homeostatic migration. Future work with our assay will aim to understand  
534 the mechanism by which *notum* facilitates homeostatic migration and wound induced  
535 migration.

536

537 **Conservation of EMT-TF function and the potential to study processes relevant to**  
538 **tumor invasion**

539 The fact that cells appear to migrate individually and that in migratory regions increased  
540 numbers of cells have extended cell processes suggested molecular mechanisms  
541 associated with EMT may regulate migration. In order to begin to test this possibility  
542 we investigated the function of two planarian *Snail* family transcription factors and a  
543 planarian ortholog of *zeb-1*, as these are conserved positive regulators of cell migration  
544 during EMT, required to down regulate the expression of genes that encode proteins  
545 that maintain cell-cell contacts, like E-cadherin (Thiery and Sleeman, 2006). Enhanced  
546 *snail* gene expression has reported in several different cancer types including ovarian  
547 carcinoma (Davidson et al., 2012), breast tumours (Blanco et al., 2002; Elloul et al.,  
548 2005); gastric cancers (Peng et al., 2014; Rosivatz et al., 2002); hepatocellular  
549 carcinomas (Miyoshi et al., 2005; Sugimachi et al., 2003); colon cancers (Pálmer et al.,  
550 2004) and synovial sarcomas (Saito et al., 2004). Overexpression or down regulation of  
551 *Snail* has shown to modulate invasiveness and metastasis in in vitro cancer cell culture  
552 studies (Adhikary et al., 2014; Belgiovine et al., 2016; Fan et al., 2012; Horvay et al.,

553 2015; Sharili et al., 2013; Smith et al., 2014; Villarejo et al., 2015). Similarly, *zebl*  
554 over-activity has also been implicated in tumorigenesis. These reports clearly suggest  
555 that EMT-TFs are key players in cancer invasion and metastasis.

556 Within the context of our assay RNAi of all three of these genes led to failure in cell  
557 migration and we were able to clearly observe decrease in cells showing extended cell  
558 processes, indicative of migratory morphology. Our data confirm the role of EMT-TFs  
559 in controlling migration in the context for our assay and suggest we can use this as a  
560 basis for studying EMT related processes in planarians. By combining functional  
561 approaches with expression screens starting with planarian homologs of EMT-related  
562 transcription factor regulators and known upstream EMT regulatory signals, we will be  
563 able to find out more about EMT in the context of tissue homeostasis, regeneration and  
564 adult stem cell activity.

565

## 566 **EXPERIMENTAL PROCEDURES**

567

### 568 **Planarian culture**

569 A *Schmidtea mediterranea* asexual strain was cultured and maintained in 0.5% instant  
570 ocean water in the dark at 20°C. Animals were starved at least 7 days before using for  
571 experiments.

572

### 573 **X-ray irradiation, and design of shield**

574 Irradiations were performed using a Comet MXR-321 x-ray set operated at 225 kVp,  
575 17mA with a 0.5 mm aluminium filter. The X-ray field is collimated to 40 mm x 20 mm  
576 with a 6.1 mm thick lead disc positioned centrally, directly above the X-ray tube focal  
577 spot and supported within an aluminium frame. The removable central shielded area is  
578 achieved using a 0.8 mm wide, 6.1 mm thick lead strip spanning the long axis of the

579 collimated field, this sits slightly proud of the main lead collimator so that it is in  
580 contact with the base of the Petri dish. When in position, the worms are irradiated at a  
581 dose rate of 23 Gy/min, reducing to ~ 1 Gy/min underneath the shielded region. The  
582 variation in dose distribution across the strip is shown in supplementary figure 1C. The  
583 circular hole in the top aluminium plate corresponds to the outside diameter of the Petri  
584 dish and enables dishes to be positioned quickly and reproducibly. Thin strips of  
585 materials such as tungsten or tantalum could be used to replace the lead strip to achieve  
586 thinner shielded regions if required.

587

### 588 **Dosimetry**

589 Dose rate measurements and spatial characterization of the treatment field was  
590 performed using Gafchromic EBT3 film (International Specialty products, Wayne, NJ)  
591 placed in the base of an empty 60 mm Petri dish. Twenty-four hours following exposure  
592 the EBT3 film was scanned in transmission mode at 48 bit RGB (16 bits per colour)  
593 with 300 dpi resolution using a flatbed scanner (Epson Expression 10000XL). A  
594 template was used to position the film within the scanner and the scanning direction  
595 was kept constant with respect to the film orientation, as recommended in the  
596 manufacturer's guidelines. The dose was calculated using the optical density of the red  
597 channel and corrected using the optical density of the blue channel in order to  
598 compensate for small non-uniformities in the film which cause false apparent variations  
599 in dose (as described in the technical brief: *Gafchromic EBT2 Self-developing film for*  
600 *radiotherapy dosimetry*). The batch of EBT3 film was calibrated following the  
601 recommendations of the report of AAPM Task Group 61 (Ma et al., 2001).

602

### 603 **Shielded irradiation**



604 Up to 20 size-matched planarians (3 to 4 mm) were anesthetized in ice cold 0.2%  
605 chloretone and aligned on 60mm Petri dish (Guedelhofer and Sánchez Alvarado,  
606 2012b). Anterior tip of all worms were aligned in a perfect line to keep the absolute  
607 migratory distance (distance between tip of the head and shielded region) fixed. Petri  
608 dish is pre-marked with a line at bottom denoting the place and dimensions (length and  
609 thickness) of the shield strip. Excess liquid is removed to minimize movement of  
610 worms during at the time of irradiation. Petri dish containing worms is then placed on to  
611 the shield of bottom source X-ray irradiator. Care is taken to perfectly match the  
612 position of shield trip and line marked on Petri dish to ascertain the exact region of the  
613 worm to be shielded. 30Gy X-ray (225kV for 1 min 18 seconds) is used for irradiation.  
614 Once irradiation is over, planarians were immediately washed with instant ocean water  
615 and transferred into fresh instant ocean water and incubated in dark at 20°C.

616

#### 617 **WFISH, immunostaining and imaging**

618 Whole mount fluorescent in-situ hybridization was performed as described previously  
619 (Currie et al., 2016; King and Newmark, 2013). H3ser10p rabbit monoclonal antibody  
620 from Millipore (04–817) was used for immunostaining (Felix and Aboobaker, 2010).  
621 Confocal imaging was done with Olympus FV1000 and Zeiss 880 Airyscan  
622 microscope. Bright field images were taken with Zeiss Discovery V8 from Carl Zeiss  
623 using Canon 1200D camera. Images were processed with Fiji and Adobe Photoshop.  
624 ZEN 2.1 (blue edition) software from Carl Zeiss was used to construct 3D images of  
625 cells. All measurements and quantifications were done with Fiji and Adobe Photoshop.  
626 Significance was determined by unpaired 2-tailed Student's t-test.

627

#### 628 **Gene cloning and RNAi**

629 Planarian genes were cloned into the pPR-T4P plasmid vector containing opposable T7  
630 RNA polymerase promoters (kind gift from Jochen Rink). The cloned vectors were then  
631 used for in vitro dsRNA synthesis and probe synthesis as described previously (King  
632 and Newmark, 2013; Rouhana et al., 2013). The primers used to generate dsRNA  
633 template from genes were as follows:

634 *mmpa* (GenBank: HE577120.1): Fw 5'- ATCCTGATTACGGCTCCAA-3' and Re 5'-  
635 TTTATTGGGGGTGCAACTGT-3'

636 *β1-integrin* (GenBank: KU961518.1): Fw 5'-GAACTCAACACACAACGCC-3' and  
637 Re 5'-TCTCGACAGGGAACAATGGC-3'

638 *snail-1* (GenBank: XXXXX): Fw 5'-AGCAATCAATCCTAAAGTCG-3' and Re 5'-  
639 CGATAGATTCTTCCACGGAG-3'

640 *snail-2* (GenBank: KJ934814.1): Fw 5'-GTTATCAAGCCAGACCTTCA-3' and Re  
641 5'-GTTTGACTTGTGAATGGGTC-3'

642 *zeb-1* (GenBank: XXXXX): Fw 5'-TCGTACCCTCATCTACCGCA-3' and Re 5'-  
643 GGGTTTCTCTCCGCTGTGAA-3'

644 Previously described sequence regions were used for dsRNA synthesis of *wnt1*  
645 (Petersen and Reddien, 2009) and *notum* (Petersen and Reddien, 2011). Reported  
646 sequences were used for riboprobe synthesis of *smedwi-1* (Reddien et al., 2005), *prog-1*  
647 (Eisenhoffer et al., 2008), *agat-1* (Eisenhoffer et al., 2008), zeta pool (van Wolfswinkel  
648 et al., 2014), and sigma pool (van Wolfswinkel et al., 2014). To generate probes for  
649 *mmpa*, *β1-integrin*, *snail-1*, *snail-2* and *zeb-1* the same regions of their respective  
650 dsRNA were used. For knockdown of genes animals were injected with 3 x 32nl of  
651 dsRNA 6 times over 2 weeks. If worms need to be used for shielded irradiation after  
652 RNAi, a 1-day gap was kept between last RNAi injection and the shielded irradiation.

653

654 **SUPPLEMENTAL INFORMATION**

655

656 Supplemental Information includes six supplemental figures.

657

## 658 **AUTHOR CONTRIBUTIONS**

659

660 PA and AAA designed the experiments. PA, EA, NK performed the experiments. JT

661 and MH helped with designing X-ray shield and performing X-ray shielded irradiations.

662 PA and AAA wrote the manuscript.

663

## 664 **ACKNOWLEDGMENTS**

665

666 We thank all members of the Aboobaker lab past and present for discussions and

667 reagent sharing. The work of PA, EA, NK, AAA is funded by the MRC (grant number

668 MR/M000133/1), BBSRC (grant number BB/K007564/1), the John Fell Fund Oxford

669 University Press (OUP), and a small grant from the CRUK Oxford Centre. NK is

670 funded by a Marie Curie Sklodowska fellowship funded by Horizon 2020. MH and JT

671 acknowledge funding from the Funding from Medical Research Council Strategic

672 Partnership Funding (MC-PC-12004) for the CRUK/MRC Oxford Institute for

673 Radiation Oncology is gratefully acknowledged.

674

## 675 **REFERENCES**

676

677 Adhikary, A., Chakraborty, S., Mazumdar, M., Ghosh, S., Mukherjee, S., Manna, A.,

678 Mohanty, S., Nakka, K.K., Joshi, S., De, A., et al. (2014). Inhibition of epithelial to

679 mesenchymal transition by E-cadherin up-regulation via repression of slug transcription

680 and inhibition of E-cadherin degradation: dual role of scaffold/matrix attachment

681 region-binding protein 1 (SMAR1) in breast cancer cells. *J. Biol. Chem.* 289, 25431–  
682 25444.

683 Bardeen, C.R., and Baetjer, F.H. (1904). The inhibitive action of the Roentgen rays on  
684 regeneration in planarians. *J. Exp. Zool.* 1, 191–195.

685 Batlle, E., Sancho, E., Francí, C., Domínguez, D., Monfar, M., Baulida, J., and García  
686 De Herreros, A. (2000). The transcription factor snail is a repressor of E-cadherin gene  
687 expression in epithelial tumour cells. *Nat. Cell Biol.* 2, 84–89.

688 Belgiovine, C., Chiesa, G., Chiodi, I., Frapolli, R., Bonezzi, K., Taraboletti, G.,  
689 D’Incalci, M., and Mondello, C. (2016). Snail levels control the migration mechanism  
690 of mesenchymal tumor cells. *Oncol. Lett.* 12, 767–771.

691 Blanco, M.J., Moreno-Bueno, G., Sarrío, D., Locascio, A., Cano, A., Palacios, J., and  
692 Nieto, M.A. (2002). Correlation of Snail expression with histological grade and lymph  
693 node status in breast carcinomas. *Oncogene* 21, 3241–3246.

694 Bonar, N.A., and Petersen, C.P. (2017). Integrin suppresses neurogenesis and regulates  
695 brain tissue assembly in planarian regeneration. *Development* dev.139964.

696 Bradshaw, B., Thompson, K., and Frank, U. (2015). Distinct mechanisms underlie oral  
697 vs aboral regeneration in the cnidarian *Hydractinia echinata*. *Elife* 4.

698 Cano, a, Pérez-Moreno, M. a, Rodrigo, I., Locascio, A., Blanco, M.J., del Barrio, M.G.,  
699 Portillo, F., and Nieto, M. a (2000). The transcription factor snail controls epithelial-  
700 mesenchymal transitions by repressing E-cadherin expression. *Nat. Cell Biol.* 2, 76–83.

701 Colvin Wanshura, L.E., Galvin, K.E., Ye, H., Fernandez-Zapico, M.E., and Wetmore,  
702 C. (2011). Sequential activation of Snail1 and N-Myc modulates sonic hedgehog-  
703 induced transformation of neural cells. *Cancer Res.* 71, 5336–5345.

704 Currie, K.W., Brown, D.D.R., Zhu, S., Xu, C., Voisin, V., Bader, G.D., and Pearson,  
705 B.J. (2016). HOX gene complement and expression in the planarian *Schmidtea*  
706 *mediterranea*. *Evodevo* 7, 7.

- 707 Davidson, B., Tropé, C.G., and Reich, R. (2012). Epithelial-mesenchymal transition in  
708 ovarian carcinoma. *Front. Oncol.* 2, 33.
- 709 Dubois, F. (1949). Contribution á l'étude de la migration des cellules de régénération  
710 chez les Planaires dulcicoles. *Bull. Biol. Fr. Belg.* 83, 213–283.
- 711 Eisenhoffer, G.T., Kang, H., and Sánchez Alvarado, A. (2008). Molecular analysis of  
712 stem cells and their descendants during cell turnover and regeneration in the planarian  
713 *Schmidtea mediterranea*. *Cell Stem Cell* 3, 327–339.
- 714 Elloul, S., Elstrand, M.B., Nesland, J.M., Tropé, C.G., Kvalheim, G., Goldberg, I.,  
715 Reich, R., and Davidson, B. (2005). Snail, Slug, and Smad-interacting protein 1 as  
716 novel parameters of disease aggressiveness in metastatic ovarian and breast carcinoma.  
717 *Cancer* 103, 1631–1643.
- 718 Fan, F., Samuel, S., Evans, K.W., Lu, J., Xia, L., Zhou, Y., Sceusi, E., Tozzi, F., Ye,  
719 X.-C., Mani, S. a, et al. (2012). Overexpression of snail induces epithelial-mesenchymal  
720 transition and a cancer stem cell-like phenotype in human colorectal cancer cells.  
721 *Cancer Med.* 1, 5–16.
- 722 Felix, D. a, and Aboobaker, a A. (2010). The TALE class homeobox gene *Smed-prep*  
723 defines the anterior compartment for head regeneration. *PLoS Genet.* 6, e1000915.
- 724 Friedl, P., and Alexander, S. (2011). Cancer invasion and the microenvironment:  
725 plasticity and reciprocity. *Cell* 147, 992–1009.
- 726 Friedl, P., and Gilmour, D. (2009). Collective cell migration in morphogenesis,  
727 regeneration and cancer. *Nat. Rev. Mol. Cell Biol.* 10, 445–457.
- 728 Friedl, P., Locker, J., Sahai, E., and Segall, J.E. (2012). Classifying collective cancer  
729 cell invasion. *Nat. Cell Biol.* 14, 777–783.
- 730 Galliot, B. (2012). Hydra, a fruitful model system for 270 years. *Int. J. Dev. Biol.* 56,  
731 411–423.
- 732 Gehrke, A.R., and Srivastava, M. (2016). Neoblasts and the evolution of whole-body

733 regeneration. *Curr. Opin. Genet. Dev.* *40*, 131–137.

734 Geisbrecht, E.R., and Montell, D.J. (2002). Myosin VI is required for E-cadherin-  
735 mediated border cell migration. *Nat. Cell Biol.* *4*, 616–620.

736 Goichberg, P. (2016). Current Understanding of the Pathways Involved in Adult Stem  
737 and Progenitor Cell Migration for Tissue Homeostasis and Repair. *Stem Cell Rev.* *12*,  
738 421–437.

739 Guedelhofer, O.C., and Sánchez Alvarado, A. (2012a). Amputation induces stem cell  
740 mobilization to sites of injury during planarian regeneration. *Development* *139*, 3510–  
741 3520.

742 Guedelhofer, O.C., and Sánchez Alvarado, A. (2012b). Planarian immobilization,  
743 partial irradiation, and tissue transplantation. *J. Vis. Exp.* 1–7.

744 Hagedorn, E.J., Ziel, J.W., Morrissey, M.A., Linden, L.M., Wang, Z., Chi, Q., Johnson,  
745 S.A., and Sherwood, D.R. (2013). The netrin receptor DCC focuses invadopodia-driven  
746 basement membrane transmigration in vivo. *J. Cell Biol.* *201*, 903–913.

747 Hill, E.M., and Petersen, C.P. (2015). Wnt/Notum spatial feedback inhibition controls  
748 neoblast differentiation to regulate reversible growth of the planarian brain.  
749 *Development*.

750 Horvay, K., Jardé, T., Casagrande, F., Perreau, V.M., Haigh, K., Nefzger, C.M., Akhtar,  
751 R., Gridley, T., Berx, G., Haigh, J.J., et al. (2015). Snai1 regulates cell lineage  
752 allocation and stem cell maintenance in the mouse intestinal epithelium. *EMBO J.* *34*,  
753 1319–1335.

754 Isolani, M.E., Abril, J.F., Saló, E., Deri, P., Bianucci, A.M., and Batistoni, R. (2013).  
755 Planarians as a Model to Assess In Vivo the Role of Matrix Metalloproteinase Genes  
756 during Homeostasis and Regeneration. *PLoS One* *8*.

757 Kakugawa, S., Langton, P.F., Zebisch, M., Howell, S.A., Chang, T.-H., Liu, Y., Feizi,  
758 T., Bineva, G., O'Reilly, N., Snijders, A.P., et al. (2015). Notum deacylates Wnt

759 proteins to suppress signalling activity. *Nature* 519, 187–192.

760 Kalluri, R., and Weinberg, R. a (2009). Review series The basics of epithelial-  
761 mesenchymal transition. *J. Clin. Invest.* 119, 1420–1428.

762 Kao, D., Mihaylova, Y., Hughes, S., Lai, A., and Aboobaker, A. (2017). Epigenetic  
763 analyses of the planarian genome reveals conservation of bivalent promoters in animal  
764 stem cells. *bioRxiv*.

765 King, R.S., and Newmark, P. a (2013). In situ hybridization protocol for enhanced  
766 detection of gene expression in the planarian *Schmidtea mediterranea*. *BMC Dev. Biol.*  
767 13, 8.

768 Lamouille, S., Xu, J., and Derynck, R. (2014). Molecular mechanisms of epithelial-  
769 mesenchymal transition. *Nat. Rev. Mol. Cell Biol.* 15, 178–196.

770 LoCascio, S.A., Lapan, S.W., and Reddien, P.W. (2017). Eye Absence Does Not  
771 Regulate Planarian Stem Cells during Eye Regeneration. *Dev. Cell* 40, 381–391.e3.

772 Ma, C.M., Coffey, C.W., DeWerd, L.A., Liu, C., Nath, R., Seltzer, S.M., Seuntjens,  
773 J.P., and American Association of Physicists in Medicine (2001). AAPM protocol for  
774 40-300 kV x-ray beam dosimetry in radiotherapy and radiobiology. *Med. Phys.* 28,  
775 868–893.

776 Mayor, R., and Theveneau, E. (2014). The role of the non-canonical Wnt-planar cell  
777 polarity pathway in neural crest migration. *Biochem. J.* 457, 19–26.

778 Miyoshi, A., Kitajima, Y., Kido, S., Shimonishi, T., Matsuyama, S., Kitahara, K., and  
779 Miyazaki, K. (2005). Snail accelerates cancer invasion by upregulating MMP  
780 expression and is associated with poor prognosis of hepatocellular carcinoma. *Br. J.*  
781 *Cancer* 92, 252–258.

782 Mogilner, A., and Keren, K. (2009). The shape of motile cells. *Curr. Biol.* 19, R762-71.

783 Montell, D.J. (2003). Border-cell migration: the race is on. *Nat. Rev. Mol. Cell Biol.* 4,  
784 13–24.

785 Pálmer, H.G., Larriba, M.J., García, J.M., Ordóñez-Morán, P., Peña, C., Peiró, S., Puig,  
786 I., Rodríguez, R., de la Fuente, R., Bernad, A., et al. (2004). The transcription factor  
787 SNAIL represses vitamin D receptor expression and responsiveness in human colon  
788 cancer. *Nat. Med.* *10*, 917–919.

789 Peng, Z., Wang, C.-X., Fang, E.-H., Wang, G.-B., and Tong, Q. (2014). Role of  
790 epithelial-mesenchymal transition in gastric cancer initiation and progression. *World J.*  
791 *Gastroenterol.* *20*, 5403–5410.

792 Petersen, C.P., and Reddien, P.W. (2009). A wound-induced Wnt expression program  
793 controls planarian regeneration polarity. *Proc. Natl. Acad. Sci. U. S. A.* *106*, 17061–  
794 17066.

795 Petersen, C.P., and Reddien, P.W. (2011). Polarized notum activation at wounds  
796 inhibits Wnt function to promote planarian head regeneration. *Science* *332*, 852–855.

797 Reddien, P.W., Oviedo, N.J., Jennings, J.R., Jenkin, J.C., and Sánchez Alvarado, A.  
798 (2005). SMEDWI-2 is a PIWI-like protein that regulates planarian stem cells. *Science*  
799 *310*, 1327–1330.

800 Reig, G., Pulgar, E., and Concha, M.L. (2014). Cell migration: from tissue culture to  
801 embryos. *Development* *141*, 1999–2013.

802 Ridley, A.J., Schwartz, M.A., Burridge, K., Firtel, R.A., Ginsberg, M.H., Borisy, G.,  
803 Parsons, J.T., and Horwitz, A.R. (2003). Cell migration: integrating signals from front  
804 to back. *Science* *302*, 1704–1709.

805 Rosivatz, E., Becker, I., Specht, K., Fricke, E., Luber, B., Busch, R., Höfler, H., and  
806 Becker, K.-F. (2002). Differential expression of the epithelial-mesenchymal transition  
807 regulators snail, SIP1, and twist in gastric cancer. *Am. J. Pathol.* *161*, 1881–1891.

808 Rouhana, L., Weiss, J. a, Forsthoefel, D.J., Lee, H., King, R.S., Inoue, T., Shibata, N.,  
809 Agata, K., and Newmark, P. a (2013). RNA interference by feeding in vitro-synthesized  
810 double-stranded RNA to planarians: methodology and dynamics. *Dev. Dyn.* *242*, 718–



811 730.

812 Saito, T., Oda, Y., Kawaguchi, K., Sugimachi, K., Yamamoto, H., Tateishi, N., Tanaka,  
813 K., Matsuda, S., Iwamoto, Y., Ladanyi, M., et al. (2004). E-cadherin mutation and Snail  
814 overexpression as alternative mechanisms of E-cadherin inactivation in synovial  
815 sarcoma. *Oncogene* 23, 8629–8638.

816 Saló, E., and Baguñà, J. (1985). Cell movement in intact and regenerating planarians.  
817 Quantitation using chromosomal, nuclear and cytoplasmic markers. *J. Embryol. Exp.*  
818 *Morphol.* 89, 57–70.

819 Sato, K., Hiraiwa, T., Maekawa, E., Isomura, A., Shibata, T., and Kuranaga, E. (2015).  
820 Left-right asymmetric cell intercalation drives directional collective cell movement in  
821 epithelial morphogenesis. *Nat. Commun.* 6, 10074.

822 Scimone, M.L., Kravarik, K.M., Lapan, S.W., and Reddien, P.W. (2014). Neoblast  
823 Specialization in Regeneration of the Planarian *Schmidtea mediterranea*. *Stem Cell*  
824 *Reports* 3, 339–352.

825 Seebeck, F., März, M., Meyer, A.-W., Reuter, H., Vogg, M.C., Stehling, M., Mildner,  
826 K., Zeuschner, D., Rabert, F., and Bartscherer, K. (2017). Integrins are required for  
827 tissue organization and restriction of neurogenesis in regenerating planarians.  
828 *Development*.

829 Sharili, A.-S., Allen, S., Smith, K., Price, J., and McGonnell, I.M. (2013). Snail2  
830 promotes osteosarcoma cell motility through remodelling of the actin cytoskeleton and  
831 regulates tumor development. *Cancer Lett.* 333, 170–179.

832 Smith, B.N., Burton, L.J., Henderson, V., Randle, D.D., Morton, D.J., Smith, B.A.,  
833 Taliaferro-Smith, L., Nagappan, P., Yates, C., Zayzafoon, M., et al. (2014). Snail  
834 promotes epithelial mesenchymal transition in breast cancer cells in part via activation  
835 of nuclear ERK2. *PLoS One* 9, e104987.

836 Sugimachi, K., Tanaka, S., Kameyama, T., Taguchi, K., Aishima, S., Shimada, M.,

- 837 Sugimachi, K., and Tsuneyoshi, M. (2003). Transcriptional repressor snail and  
838 progression of human hepatocellular carcinoma. *Clin. Cancer Res.* 9, 2657–2664.
- 839 Tanaka, E.M., and Reddien, P.W. (2011). The cellular basis for animal regeneration.  
840 *Dev. Cell* 21, 172–185.
- 841 Tasaki, J., Uchiyama-Tasaki, C., and Rouhana, L. (2016). Analysis of Stem Cell  
842 Motility In Vivo Based on Immunodetection of Planarian Neoblasts and Tracing of  
843 BrdU-Labeled Cells After Partial Irradiation. *Methods Mol. Biol.* 1365, 323–338.
- 844 Thiery, J.P., and Sleeman, J.P. (2006). Complex networks orchestrate epithelial-  
845 mesenchymal transitions. *Nat. Rev. Mol. Cell Biol.* 7, 131–142.
- 846 Traister, A., Shi, W., and Filmus, J. (2008). Mammalian Notum induces the release of  
847 glypicans and other GPI-anchored proteins from the cell surface. *Biochem. J.* 410, 503–  
848 511.
- 849 Tu, K.C., Cheng, L.-C., T K Vu, H., Lange, J.J., McKinney, S.A., Seidel, C.W., and  
850 Sánchez Alvarado, A. (2015). Egr-5 is a post-mitotic regulator of planarian epidermal  
851 differentiation. *Elife* 4, e10501.
- 852 Vicente-Manzanares, M., Choi, C.K., and Horwitz, A.R. (2009). Integrins in cell  
853 migration--the actin connection. *J. Cell Sci.* 122, 199–206.
- 854 Villarejo, A., Molina-Ortiz, P., Montenegro, Y., Moreno-Bueno, G., Morales, S.,  
855 Santos, V., Gridley, T., Pérez-Moreno, M.A., Peinado, H., Portillo, F., et al. (2015).  
856 Loss of Snail2 favors skin tumor progression by promoting the recruitment of myeloid  
857 progenitors. *Carcinogenesis* 36, 585–597.
- 858 Witchley, J.N., Mayer, M., Wagner, D.E., Owen, J.H., and Reddien, P.W. (2013).  
859 Muscle cells provide instructions for planarian regeneration. *Cell Rep.* 4, 633–641.
- 860 Wolff, E. (1962). Recent researches on the regeneration of planaria. In “Regeneration.  
861 20th Growth Symposium” (D. Rudnick, Ed), (New York: Ronald Press), pp. 53–84.
- 862 van Wolfswinkel, J.C., Wagner, D.E., and Reddien, P.W. (2014). Single-Cell Analysis

863 Reveals Functionally Distinct Classes within the Planarian Stem Cell Compartment.

864 *Cell Stem Cell* 15, 326–339.

865 Zhang, X., Cheong, S.-M., Amado, N.G., Reis, A.H., MacDonald, B.T., Zebisch, M.,

866 Jones, E.Y., Abreu, J.G., and He, X. (2015). Notum is required for neural and head

867 induction via Wnt deacylation, oxidation, and inactivation. *Dev. Cell* 32, 719–730.

868

## 869 **FIGURE LEGENDS**

870

### 871 **Figure 1. Shielded irradiation assay setup to generate stripped worms**

872 (A) Point source X-ray irradiator with the lead shield on top and holding worms aligned

873 in a Petri dish.

874 (B) Worms anesthetized in 0.2% chloretone and aligned in a straight line on 60mm Petri

875 dish.

876 (C) Lead shield with a horizontal lead stripe in the middle.

877 (D) Wild type un-irradiated planarians showing distribution of NBs (green) and early

878 progeny (magenta).

879 (E) Striped planarians at 4 days post shielded irradiation (4dpi) showing band of stem

880 cells (green) and early progeny (magenta) restricted to the irradiation-protected region.

881 A 30 Gy X-ray dose is used.

882 (F) Gradual loss of NBs (green) and early progeny (magenta) in the non-shielded region

883 after 1 dpi, 2dpi, 3dpi and 4dpi respectively (n=10), and maintenance within the

884 shielded region.

885 See also Figure S1.

886

### 887 **Figure 2. Wound induced cell migration and characteristic extended morphology**

888 **of migrating stem cells and stem cell progeny**

889 (A) Diagrammatic model demonstrating the position of the wound and three (I, II and  
890 III) independent methods for measuring cell migration distances.

891 (B) Representative WFISH showing migration and repopulation of NBs (green) and  
892 early progeny (magenta) after shielding of across the pharynx at 1, 4, 7 and 10 days post  
893 injury (n=20 per time point). Scale bars: 500 $\mu$ m.

894 (C) Measurements of distances migrated by NBs (green) and early progeny (magenta)  
895 at 1, 4, 7 and 10 days post decapitation. Each dot represents average distance migrated  
896 by 10 most distal cells in each animal (n=25 per time point). Lines and error bars  
897 indicate mean and SD.

898 (D) Numbers of NB to early progeny ratios in the migratory region are plotted at 1, 4, 7  
899 and 10 days post decapitation (n=20 per time point). Ratio of cells in shielded region  
900 and in unexposed worms is used as a control. The results are expressed as means  $\pm$ SD.

901 (E) Quantification of NBs (magenta) and mitotic cells (green) in the migratory region  
902 following decapitation at 1, 4, 7 and 10 days (n=20 per time point). The results are  
903 expressed as means  $\pm$ SD.

904 (F) Morphology of cells within the shielded region in an uninjured worm shows very  
905 few stem cells (green) and few early progeny cells (magenta) with extended  
906 cytoplasmic projections (n=20).

907 (G) Morphology of cells within the shielded region in the decapitated worm shows few  
908 stem cells (green) and some early progeny cells (magenta) with extended cytoplasmic  
909 projections (n=20).

910 (H) Morphology of cells within the migratory region in the decapitated worm shows  
911 few stem cells (green) and many early progeny cells (magenta) with extended  
912 cytoplasmic projections (n=20).

913 (I) Quantification shows increase in number of stem cells (green) and early progeny  
914 cells (magenta) with extended processes within decapitated/migratory region as well as

915 decapitated/shielded region compared to the uninjured/shielded region (n=20 per  
916 condition). The results are expressed as means  $\pm$ SD. Student's t test: \*p<0.05.

917 (J-M) Early progeny cells (magenta) within migratory region in decapitated worms  
918 show extended processes in various directions relative to the wound. Yellow arrows  
919 indicate the direction of extended processes. Position of wound relative to cells is to the  
920 top.

921 See also Figure S2.

922

923 **Figure 3. Migration of different epidermal lineage cells shows that cells migrate in**  
924 **the specific order with most differentiated progeny to undifferentiated NBs**

925 (A) Current model of planarian epidermal lineage differentiation. Sigma class NBs give  
926 rise to zeta class NBs that produces *prog-I*<sup>+</sup> early progeny. *prog-I*<sup>+</sup> early progeny  
927 differentiate into *agat-I*<sup>+</sup> late progeny which terminally differentiate into epidermal  
928 cells.

929 (B-K) FISH showing migration of different cell types from epidermal lineage at 7dpa.  
930 *agat-I* cells (magenta) migrate way ahead of *smedwi-I* cells (green) (B, C). *prog-I* cells  
931 (magenta) migrate way ahead of *smedwi-I* cells (green) (D, E). *prog-I* cells (magenta),  
932 Zeta class cells (green) and *prog-I* + Zeta class double positive cells (white) migrate  
933 with the similar speed (F, G). *smedwi-I* zeta class cells (magenta) migrate way ahead of  
934 *smedwi-I*<sup>+</sup> zeta stem cells (white) and *smedwi-I* cells (green) (H, I). *smedwi-I*<sup>+</sup> sigma  
935 stem cells (white) and *smedwi-I* cells (green) migrate with the similar speed (J, K) (n=5  
936 per condition). White arrows indicate the examples of double positive cells. Scale bars:  
937 300 $\mu$ m for zoomed out and 100 $\mu$ m for zoomed in view.

938 (L) Measurements of distance travelled by different cell populations (*smedwi-I*<sup>+</sup> sigma  
939 class stem cells, *smedwi-I*<sup>+</sup> zeta class stem cells, *smedwi-I* zeta class cells, *prog-I* +

940 zeta class double positive cells, *prog-1* cells and *agat-1* cells) in decapitated worms at  
941 7dpa. (n=15 per condition, Student's t test: \*p<0.05)  
942 (M) Model demonstrating order in which different cells migrate following decapitation.  
943 *agat-1*, *prog-1*, *prog-1* + zeta class double positive cells migrate most anteriorly and are  
944 most distal to the shielded region. Zeta class (*smedwi-1*) cells migrate equally with  
945 *prog-1*, *prog-1* + zeta class double positive cells but are quite distant to *agat-1* cells.  
946 Zeta stem cells and sigma stem cells migrate with the slowest speed and are most  
947 proximal to the shielded region.

948

949 **Figure 4. *mmpa* and  $\beta 1$ -integrin are essential for stem cell and progeny migration**  
950 **as well as for developing extended cell morphology**

951 (A-L) FISH shows migration of stem cells (green) and early progeny (magenta) at 7dpa  
952 in *gfp(RNAi)* (A-C, G-I) worms but the migration is inhibited in *mmpa(RNAi)* (D-F) as  
953 well as in  $\beta 1$ -*integrin(RNAi)* (J-L) worms. Insets show the presence of stem cells  
954 (green) and early progeny (magenta) with extended cytoplasmic projections in  
955 migratory region of *gfp(RNAi)* worms (B, C, H, I) but are almost absent in *mmpa(RNAi)*  
956 (E, F) and  $\beta 1$ -*integrin(RNAi)* (K, L) worms (n=5).

957 (M) Measurements shows drastic decrease in the distance migrated by stem cells  
958 (green) and early progeny (magenta) at 7dpa in *mmpa(RNAi)* and  $\beta 1$ -*integrin(RNAi)*  
959 animals compared to *gfp(RNAi)* worms (n=5). Each dot represents the average distance  
960 migrated by 10 most distal cells from each animal. Lines and error bars indicate mean  
961 and SD. Student's t test: \*p<0.05.

962 (N) Quantification shows that stem cells (green) and early progeny (magenta) with  
963 extended processes are reduced significantly in *mmpa(RNAi)* and  $\beta 1$ -*integrin(RNAi)*  
964 animals in comparison with *gfp(RNAi)* animals at 7dpa (n=5). The results are expressed  
965 as means  $\pm$ SD. Student's t test: \*p<0.05.

966 See also Figure S3.

967

968 **Figure 5. Stem cells and progeny characteristically migrate in anterior direction**  
969 **even without an injury**

970 (A) Cartoon showing strategy of shielding worms at various places along the anterior-  
971 posterior axis.

972 (B-J) Bright field images of worms shielded at 3 different places, posterior (B, C),  
973 middle (E, F) and anterior (H, I) in shielded irradiation assay showing regression and  
974 recovery over the time. Bright field images show head regression in posteriorly shielded  
975 worms (B), head and tail regression in middle shielded worms (E) and tail regression in  
976 anteriorly shielded worm (H). As cells migrate and repopulate the regressed anterior  
977 and posterior regions recovered over the time in all posterior (C), middle (F) and  
978 anterior (I) shielded worms (n=20 per time point). Scale bars: 500 $\mu$ m.

979 (D, G, J) FISH showing no migration of stem cells (green) and early progeny (magenta)  
980 in posteriorly shielded worms (D) until anterior tissue regress close enough to the  
981 shielded region. Whereas, stem cells (green) and early progeny (magenta) migrate as  
982 well as repopulate towards the anterior direction in middle (G) and anteriorly (J)  
983 shielded worms (n=20 per time point). Migration takes less time in anteriorly placed  
984 shields. Scale bars: 500 $\mu$ m.

985 (K) Measurements of distance migrated by stem cells (green) and early progeny  
986 (magenta) in the worms shielded irradiated at different places along AP axis. Each dot  
987 represent average distance migrated by 10 most distal cells in each animal (n=6).

988 (L) Model showing gradient of signal (orange) form head tip to up to ~1300 $\mu$ m towards  
989 posterior.

990

991 **Figure 6. Effect of *notum* RNAi and *wnt1* RNAi on cell migration**

992 (A-I) FISH showing migration of stem cells (green) and early progeny (magenta) at 7  
993 days post decapitation in *gfp(RNAi)* (A-C) animals and is unaffected in *notum(RNAi)*  
994 (D-F) and *wnt1(RNAi)* (G-I) animals. Insets shows that stem cells (green) and early  
995 progeny (magenta) in migratory region from *gfp(RNAi)* (B, C), *notum(RNAi)* (E-F) and  
996 *wnt1(RNAi)* (H-I) are able to form extended processes.  
997 (J) Measurements show that distance migrated by stem cells (green) and early progeny  
998 (magenta) at 7 dpa in *gfp(RNAi)*, *notum(RNAi)* and *wnt1(RNAi)* animals is equal (n=5).  
999 Each dot represents the average distance migrated by 10 most distal cells from each  
1000 animal. Lines and error bars indicate mean and SD. Student's t test used for analysis.  
1001 (K) Quantification shows that the number of stem cells (green) and early progeny  
1002 (magenta) with extended processes is unaffected in *notum(RNAi)* and *wnt1(RNAi)*  
1003 animals compared to *gfp(RNAi)* animals (n=5). The results are expressed as means  $\pm$ SD.  
1004 Student's t test used for analysis.  
1005 (L-Q) FISH showing reduced migration of stem cells (green) and early progeny  
1006 (magenta) at 10dpi in intact *notum(RNAi)* (O-Q) animals compared to intact *gfp(RNAi)*  
1007 (L-N) animals. Insets show extended morphology of stem cells (green) and early  
1008 progeny (magenta) in migratory region (M, N, P, Q).  
1009 (R) Measurements show that distance migrated by stem cells (green) and early progeny  
1010 (magenta) at 10dpi in *notum(RNAi)* animals is significantly reduced compared to  
1011 *gfp(RNAi)* animals (n=5). Each dot represents the average distance migrated by 10 most  
1012 distal cells from each animal. Lines and error bars indicate mean and SD. Student's t  
1013 test: \*p<0.05.  
1014 (S) Quantification shows that the number of stem cells (green) and early progeny  
1015 (magenta) with extended processes is unaffected in *notum(RNAi)* compared to  
1016 *gfp(RNAi)* animals (n=5). The results are expressed as means  $\pm$ SD. Student's t test used  
1017 for analysis.



1018 See also Figure S4.

1019

1020 **Figure 7. Snail family genes control stem cell and progeny migration**

1021 (A-O) FISH shows migration of stem cells (green) and early progeny (magenta) at 7dpa  
1022 in *gfp(RNAi)* (A-C, J-L) worms but the migration is inhibited in *snail-1(RNAi)* (D-F),  
1023 *snail-2(RNAi)* (G-I) as well as in *zeb-1(RNAi)* (M-O) worms. Insets show the presence  
1024 of stem cells (green) and early progeny (magenta) with extended cytoplasmic  
1025 projections in migratory region of *gfp(RNAi)* worms (B, C, K, L) but are reduced in  
1026 *snail-1(RNAi)* (E, F), *snail-2(RNAi)* (H-I) and *zeb-1(RNAi)* (N-O) worms (n=5).

1027 (P) Measurements shows drastic decrease in the distance migrated by stem cells (green)  
1028 and early progeny (magenta) at 7dpa in *snail-1(RNAi)*, *snail-2(RNAi)* and *zeb-1(RNAi)*  
1029 animals compared to *gfp(RNAi)* (n=5). Each dot represents the average distance  
1030 migrated by 10 most distal cells from each animal. Lines and error bars indicate mean  
1031 and SD. Student's t test: \*p<0.05.

1032 (Q) Quantification shows that stem cells (green) and early progeny (magenta) with  
1033 extended processes are reduced significantly in *snail-1(RNAi)*, *snail-2(RNAi)* and *zeb-*  
1034 *1(RNAi)* animals in comparison with *gfp(RNAi)* at 7dpa (n=5). The results are expressed  
1035 as means  $\pm$ SD. Student's t test: \*p<0.05.

1036 See also Figure S5 and S6.

1037

1038 **SUPPLEMENTARY FIGURE LEGENDS**

1039

1040 **Figure S1. Parts and dimensions of lead shield assembly**

1041 (A) Lead strip and lead shield are assembled with aluminium support which further  
1042 covered with aluminium disc to support Petri dish in the final lead shield assembly.

1043 (B) Dimensions of lead shield and lead strip from top and side view. Unit: mm.

1044 (C) Dose distribution across the lead strip showing greater than 95% attenuation of X-  
1045 ray dose under the shield protected region.

1046

1047 **Figure S2. General features of cell migration and different shapes of migrating and**  
1048 **non-migrating cells**

1049 (A) FISH showing distribution of stem cells (green) in intact wild type worm. Stem  
1050 cells are absent in the pharynx region, in brain region and region anterior to  
1051 photoreceptors (\*). Scale bar: 500 $\mu$ m.

1052 (B) FISH showing that stem cells (green) are absent in the early regenerative blastema  
1053 in a tail fragment regenerating at 3dpa (n=5). Scale bar: 200 $\mu$ m.

1054 (C) H3P immunostaining shows increase in mitotic cells (yellow) in the migratory  
1055 region in decapitated animals over the time course, 1dpa, 4dpa, 7dpa and 10dpa (n=5  
1056 per time point). Scale bar: 500 $\mu$ m.

1057 (D) Graph showing increasing distance of mitotic cells (magenta dots) from the  
1058 shielded region over the time course, 1dpa, 4dpa, 7dpa and 10dpa (n=5 per time point).  
1059 Each dot represents the distance of individual H3P cell from the shielded region. 5 most  
1060 distal H3P cells were considered for measurements from each animal. Lines and error  
1061 bars indicate mean and SD.

1062 (E, F) Stem cells (green) and early progeny (magenta) show directional migration  
1063 towards the site of poking (E) and notch (F).

1064 (G) Stem cells (green) and early progeny (magenta) from the dorsal side migrate more  
1065 rapidly than the ventral side. Scale bar: 100 $\mu$ m.

1066 (H) Measurements of distance migrated by stem cells (green) and early progeny  
1067 (magenta) from dorsal and ventral side in decapitated animal at 4dpa. Each dot  
1068 represents average the distance migrated by 10 most distal cells in an animal (n=5).  
1069 Lines and error bars indicate mean and SD.

1070 (I) Montage showing migrating stem cells (green) in different planes from dorsal to  
1071 ventral side (1 to 6).

1072 (J-K) Different morphology of stem cells (green) (J) and early progeny (magenta) (K)  
1073 without and with extended processes.

1074

1075 **Figure S3. Regenerative morphology of RNAi animals and expression patterns of**  
1076 ***mmpa* and  $\beta 1$ -*integrin***

1077 (A) Head, Trunk and Tail fragments regenerated at 11 days post amputation following  
1078 *gfp(RNAi)*, *mmpa(RNAi)* and  *$\beta 1$ -integrin(RNAi)*. (n=10)

1079 (B) Rescue and regeneration of *gfp(RNAi)*, *mmpa(RNAi)* and  *$\beta 1$ -integrin(RNAi)* worms  
1080 following shielded irradiation and decapitation. (n=30)

1081 (C-D) Expression (C) and FPKM (D) profile of *mmpa* in X1, X2 and Xins cell  
1082 population.

1083 (E) FISH showing whole body expression pattern of *mmpa*.

1084 (F-G) FISH showing expression of *mmpa* in *smewi-1<sup>+</sup>* NBs (F) and *prog-1<sup>+</sup>* progeny

1085 (G) at 2dpa. Around 3% *smewi-1<sup>+</sup>* NBs express *mmpa* and no detectable expression of  
1086 *mmpa* found in *prog-1<sup>+</sup>* progeny. Scale bars: 20 $\mu$ m

1087 (H-I) Expression (H) and FPKM (I) profile of  *$\beta 1$ -integrin* in X1, X2 and Xins cell  
1088 population.

1089 (J) FISH showing whole body expression pattern of  *$\beta 1$ -integrin*.

1090 (K-L) FISH showing expression of  *$\beta 1$ -integrin* in *smewi-1<sup>+</sup>* NBs (K) and *prog-1<sup>+</sup>*

1091 progeny (L) at 2dpa. Around 92% *smewi-1<sup>+</sup>* NBs and 33% *prog-1<sup>+</sup>* progeny express  
1092  *$\beta 1$ -integrin*.

1093 (M) FISH shows stem cells (green) and early progeny (magenta) migrate and repopulate

1094 the entire migratory region at 15dpa in *gfp(RNAi)* animals but the migration is inhibited

1095 in *mmpa(RNAi)* and  *$\beta 1$ -integrin(RNAi)* worms that leads to regression of anterior tissue.

1096 (N) Measurements shows drastic decrease in the distance migrated by stem cells (green)  
1097 and early progeny (magenta) at 15dpa in *mmpa(RNAi)* and  *$\beta$ 1-integrin(RNAi)* animals  
1098 compared to *gfp(RNAi)* worms (n=5). Each dot represents the average distance migrated  
1099 by 10 most distal cells from each animal. Lines and error bars indicate mean and SD.  
1100 Student's t test: \*p<0.05.

1101

1102 **Figure S4. Regenerative phenotype of *notum* and *wnt1* RNAi animals**

1103 (A) Head, Trunk and Tail fragments regenerated at 11 days post amputation following  
1104 *gfp(RNAi)*, *notum(RNAi)* and *wnt1(RNAi)*. (n=10)

1105 (B) Rescue and regeneration of *gfp(RNAi)*, *notum(RNAi)* and *wnt1(RNAi)* worms  
1106 following shielded irradiation and decapitation. (n=30)

1107 (C) Rescue of intact uninjured animals in *gfp(RNAi)* and *notum(RNAi)* worms following  
1108 shielded irradiation. (n=30)

1109 (D) FISH shows stem cells (green) and early progeny (magenta) migrate anteriorly and  
1110 repopulate almost entire migratory region at 20dpi in *gfp(RNAi)* animals but the  
1111 migration is inhibited in *notum(RNAi)* worms that leads to regression of anterior tissue.

1112 (E) Measurements shows drastic decrease in the distance migrated by stem cells (green)  
1113 and early progeny (magenta) at 20dpi in *notum(RNAi)* compared to *gfp(RNAi)* worms  
1114 (n=5). Each dot represents the average distance migrated by 10 most distal cells from  
1115 each animal. Lines and error bars indicate mean and SD. Student's t test: \*p<0.05.

1116

1117 **Figure S5. Regenerative morphology of RNAi animals and expression patterns of**  
1118 ***snail-1* and *snail-2***

1119 (A) Head, Trunk and Tail fragments regenerated at 11 days post amputation following  
1120 *gfp(RNAi)*, *snail-1(RNAi)* and *snail-2(RNAi)*. (n=10)

1121 (B) Rescue and regeneration of *gfp(RNAi)*, *snail-1(RNAi)* and *snail-2(RNAi)* worms  
1122 following shielded irradiation and decapitation. (n=30)  
1123 (C-D) Expression (C) and FPKM (D) profile of *snail-1* in X1, X2 and Xins cell  
1124 population.  
1125 (E) FISH showing whole body expression pattern of *snail-1*.  
1126 (F-G) FISH showing expression of *mmpa* in *smcdwi-1<sup>+</sup>* NBs (F) and *prog-1<sup>+</sup>* progeny  
1127 (G) at 2dpa. Around 87% *smcdwi-1<sup>+</sup>* NBs express *snail-1* and very little (~1%)  
1128 expression of *snail-1* found in *prog-1<sup>+</sup>* progeny. Scale bars: 20µm.  
1129 (H-I) Expression (H) and FPKM (I) profile of *snail-2* in X1, X2 and Xins cell  
1130 population.  
1131 (J) FISH showing whole body expression pattern of *snail-2*.  
1132 (K-L) FISH showing expression of *snail-2* in *smcdwi-1<sup>+</sup>* NBs (K) and *prog-1<sup>+</sup>* progeny  
1133 (L) at 2dpa. Around 93% *smcdwi-1<sup>+</sup>* NBs and less than 3% *prog-1<sup>+</sup>* progeny express  
1134 *snail-2*. Scale bars: 20µm.  
1135 (M) FISH shows stem cells (green) and early progeny (magenta) migrate and repopulate  
1136 the entire migratory region at 15dpa in *gfp(RNAi)* animals but the migration is inhibited  
1137 in *snail-1(RNAi)* and *snail-2(RNAi)* worms that leads to regression of anterior tissue.  
1138 (N) Measurements shows drastic decrease in the distance migrated by stem cells (green)  
1139 and early progeny (magenta) at 15dpa in *snail-1(RNAi)* and *snail-2(RNAi)* animals  
1140 compared to *gfp(RNAi)* worms (n=5). Each dot represents the average distance migrated  
1141 by 10 most distal cells from each animal. Lines and error bars indicate mean and SD.  
1142 Student's t test: \*p<0.05.

1143

1144 **Figure S6. Effect of *zeb-1* RNAi on regeneration and its expression in different cell**  
1145 **population**

1146 (A) Head, Trunk and Tail fragments regenerated at 11 days post amputation following  
1147 *gfp(RNAi)* and *zeb-1(RNAi)* animals. (n=10)

1148 (B) Rescue and regeneration of *gfp(RNAi)* and *zeb-1(RNAi)* worms following shielded  
1149 irradiation and decapitation. (n=30)

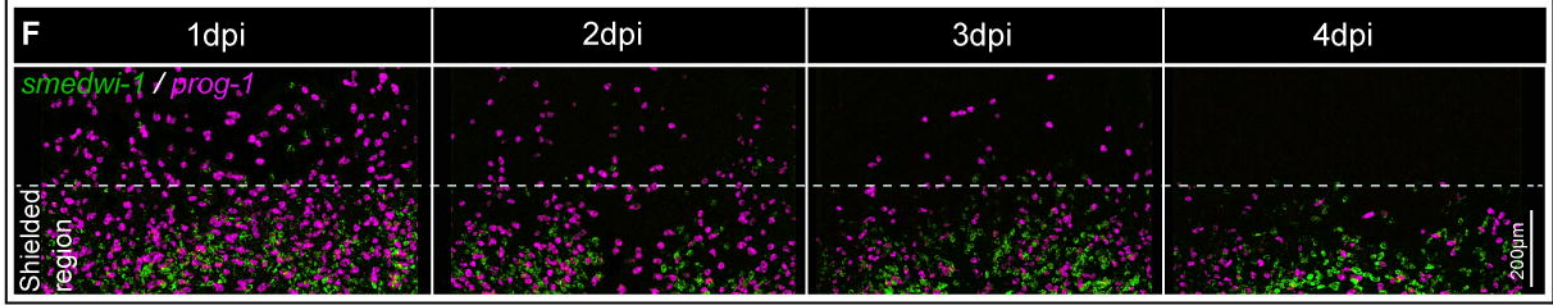
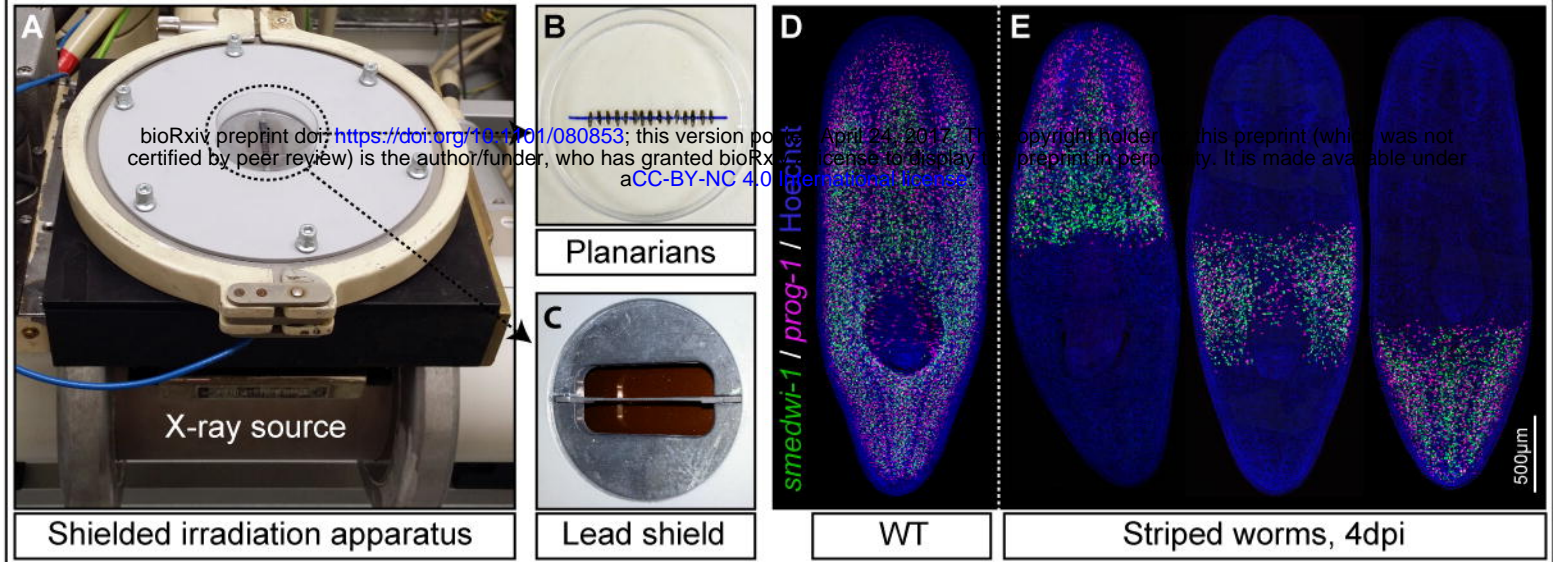
1150 (C-D) Expression (C) and FPKM (D) profile of *zeb-1* in X1, X2 and Xins cell  
1151 population.

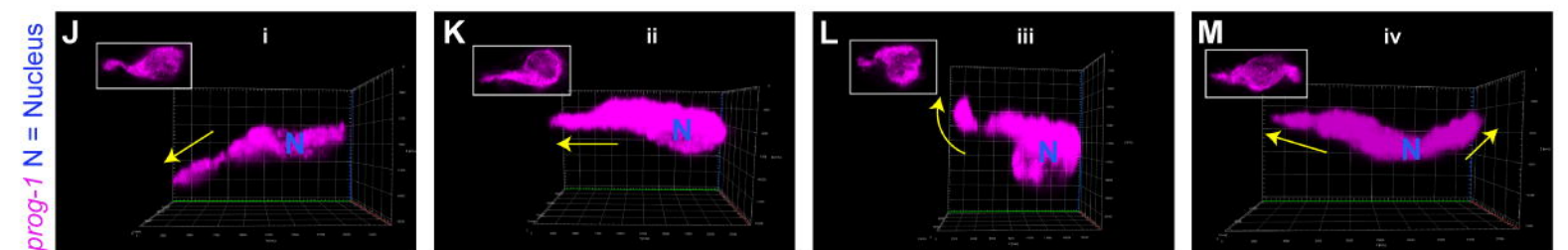
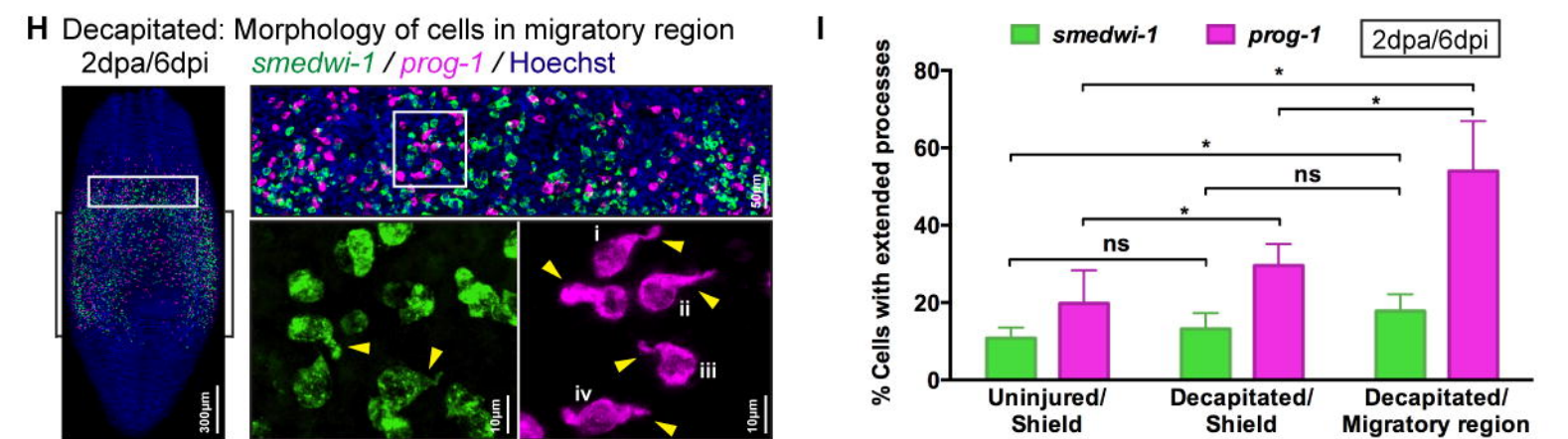
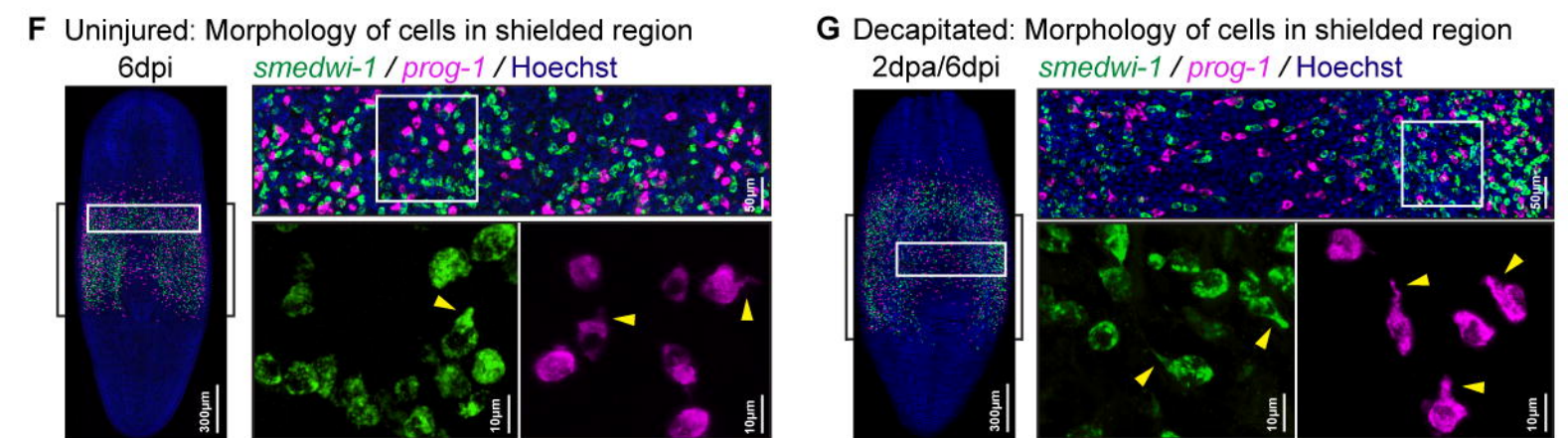
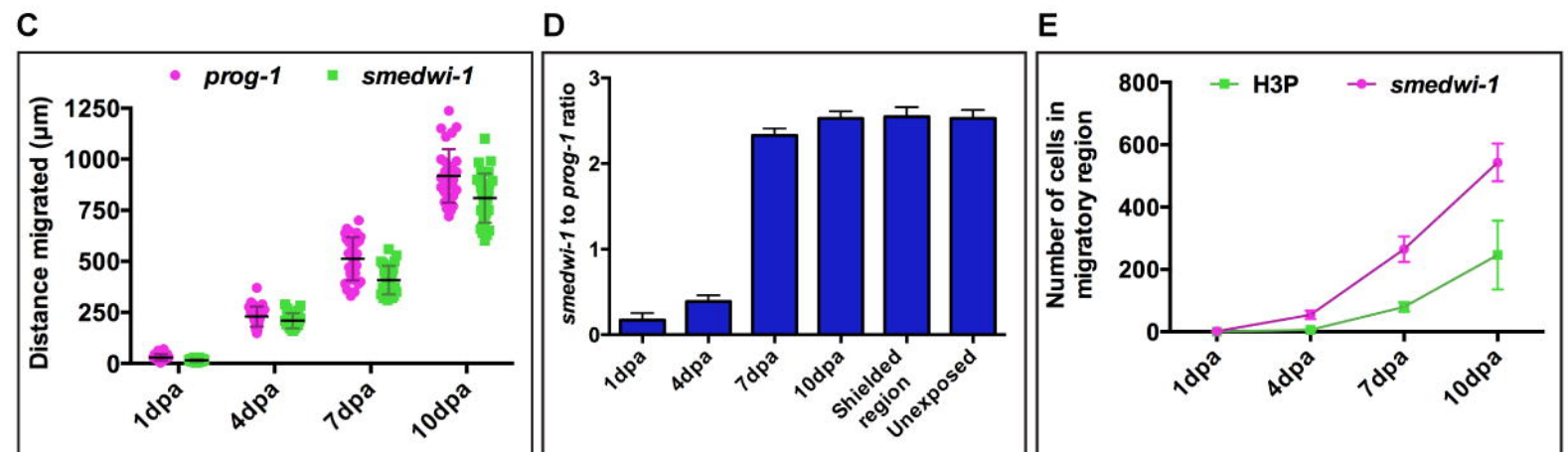
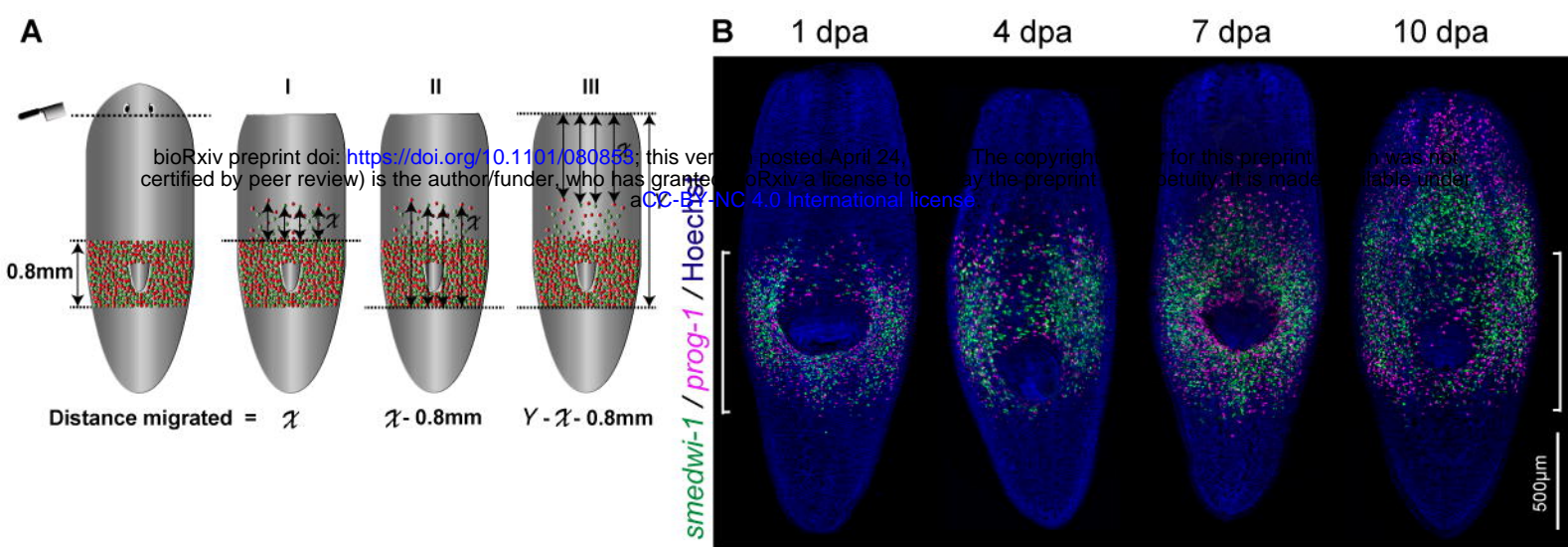
1152 (E) FISH showing whole body expression pattern of *zeb-1*.

1153 (F-G) FISH showing expression of *zeb-1* in *smcdwi-1<sup>+</sup>* NBs (F) and *prog-1<sup>+</sup>* progeny  
1154 (G) at 2dpa. Around 8% *smcdwi-1<sup>+</sup>* NBs express *zeb-1* and very little (~1%) expression  
1155 of *zeb-1* found in *prog-1<sup>+</sup>* progeny. Scale bars: 20µm.

1156 (H) FISH shows stem cells (green) and early progeny (magenta) migrate and repopulate  
1157 the entire migratory region at 15dpa in *gfp(RNAi)* animals but the migration is inhibited  
1158 in *zeb-1(RNAi)* worms that leads to regression of anterior tissue.

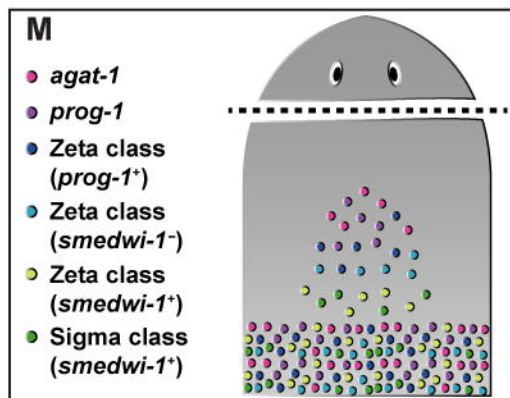
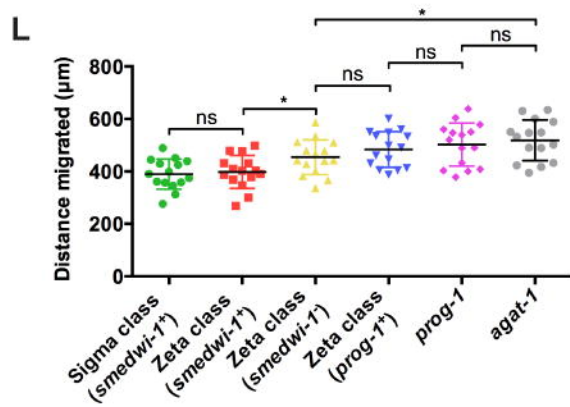
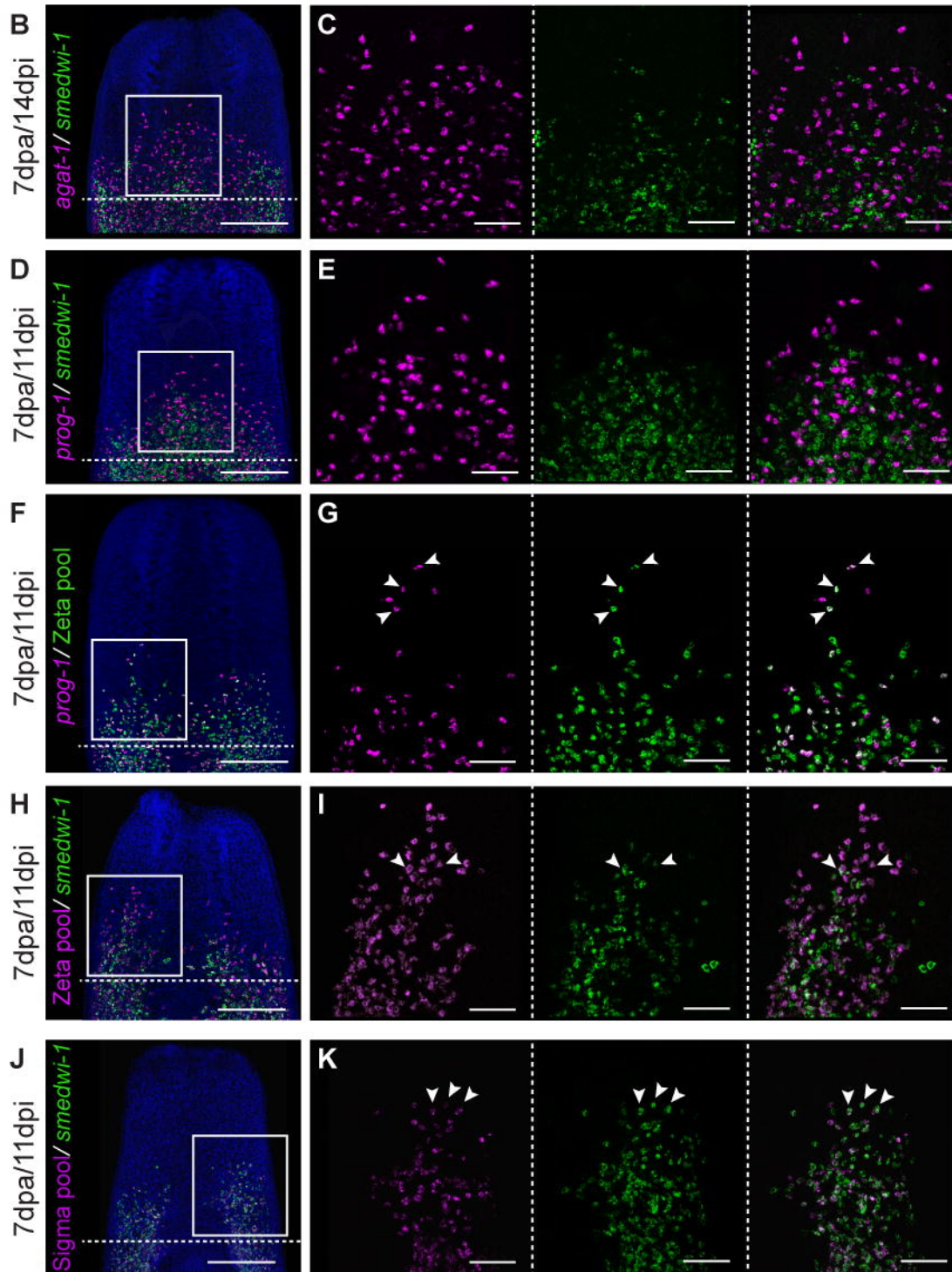
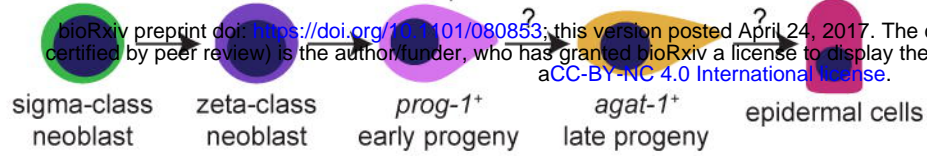
1159 (I) Measurements shows drastic decrease in the distance migrated by stem cells (green)  
1160 and early progeny (magenta) at 15dpa in *zeb-1(RNAi)* animals compared to *gfp(RNAi)*  
1161 worms (n=5). Each dot represents the average distance migrated by 10 most distal cells  
1162 from each animal. Lines and error bars indicate mean and SD. Student's t test: \*p<0.05.  
1163  
1164

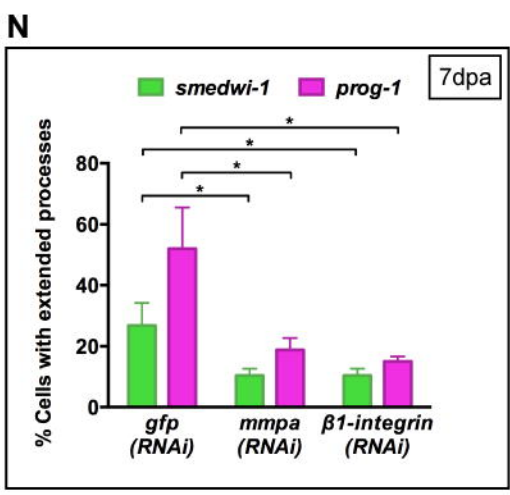
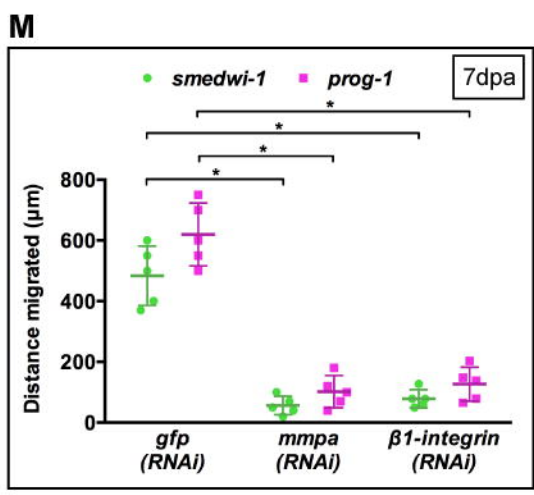
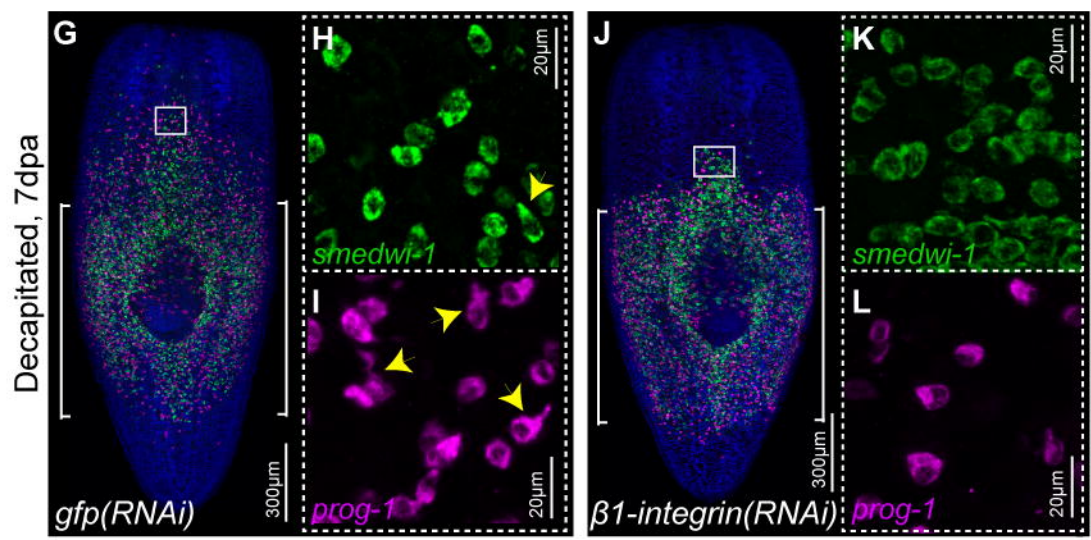
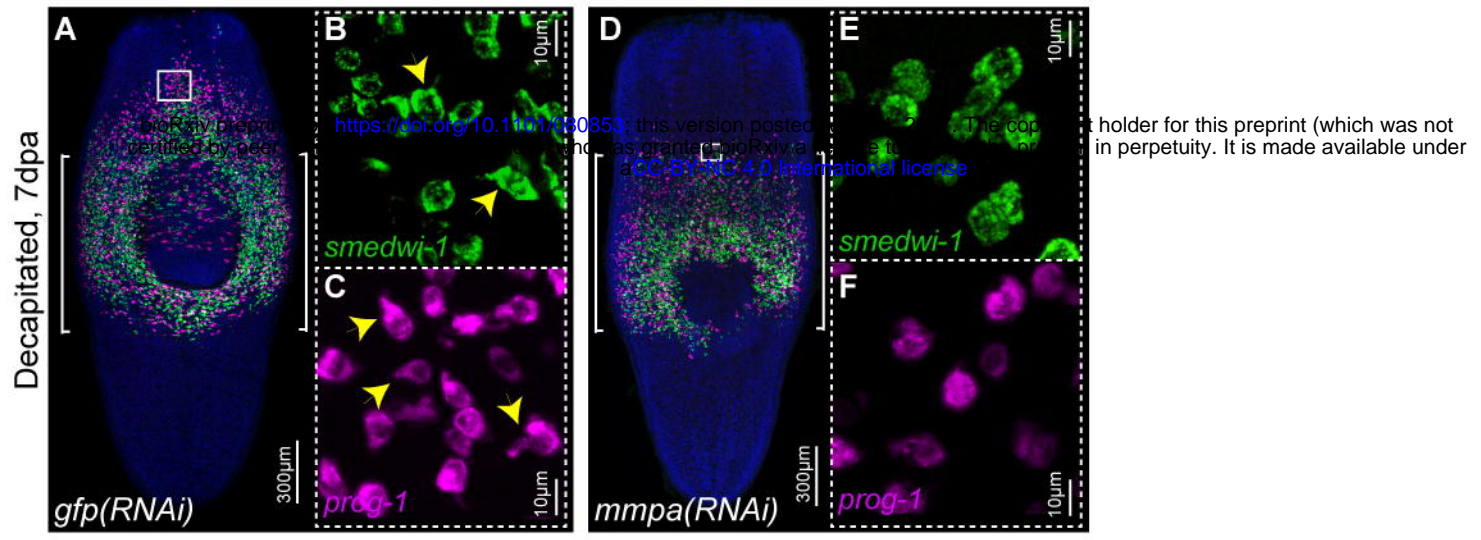


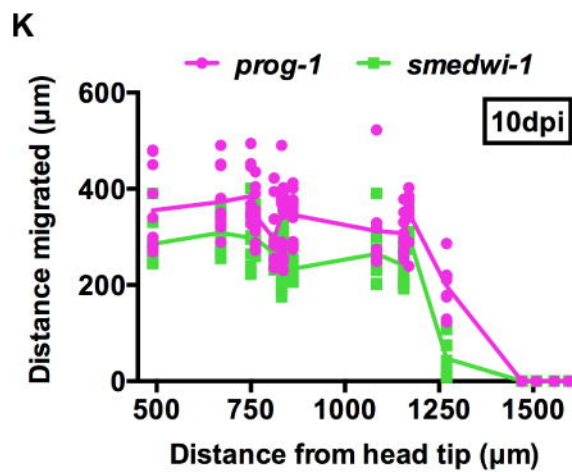
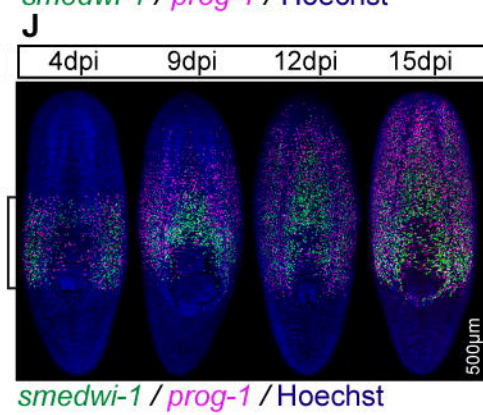
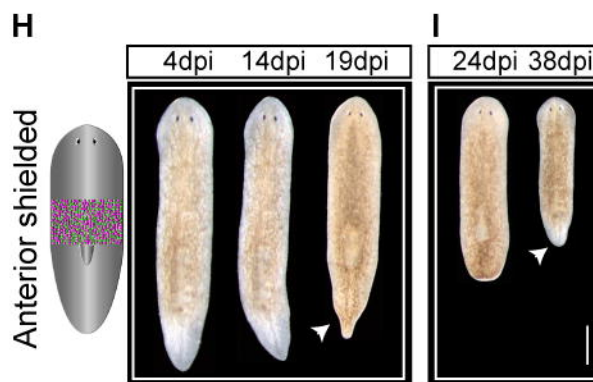
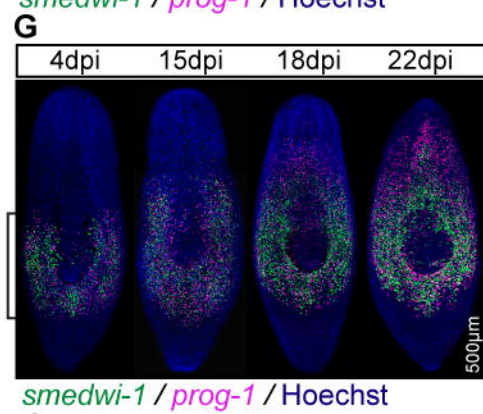
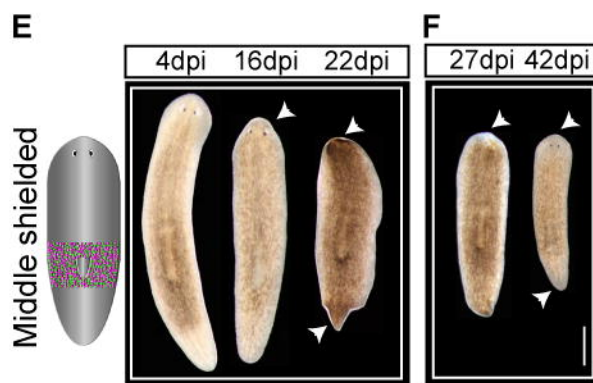
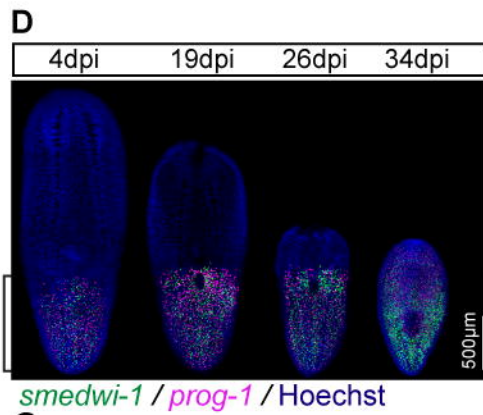
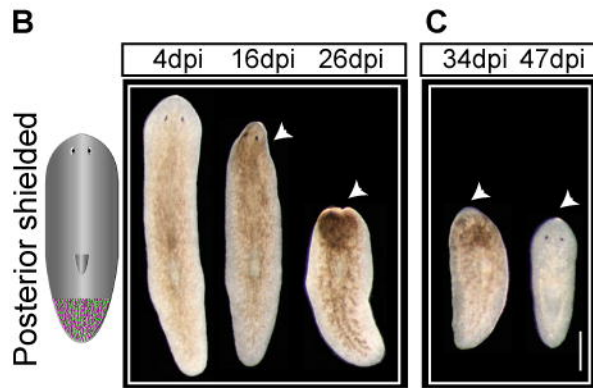
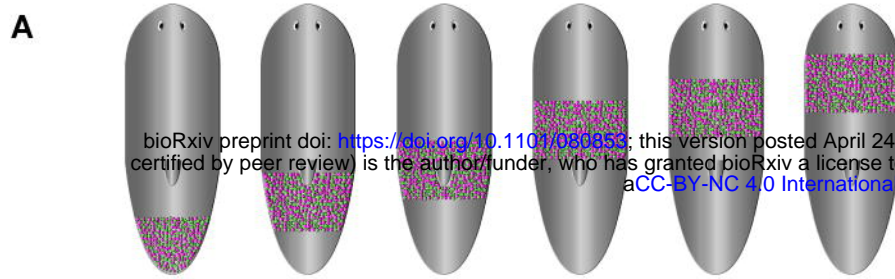




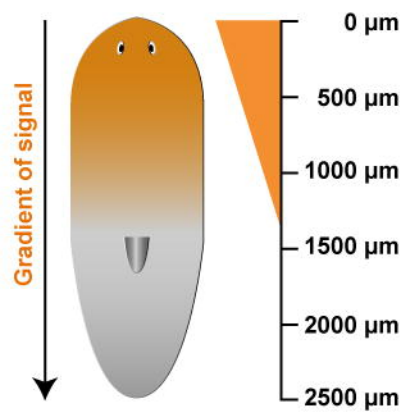
# A Planarian epidermal lineage



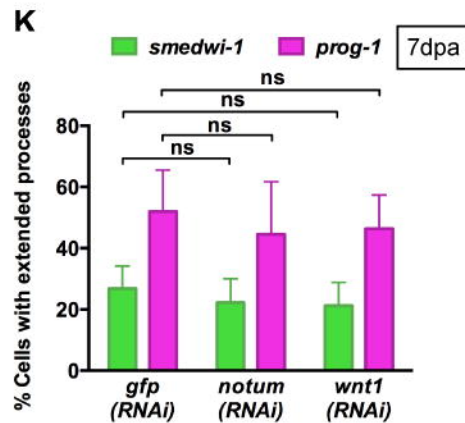
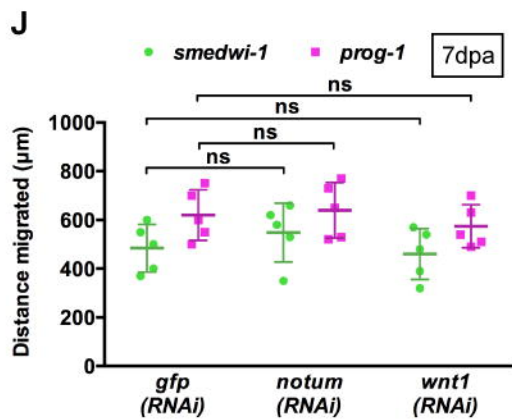
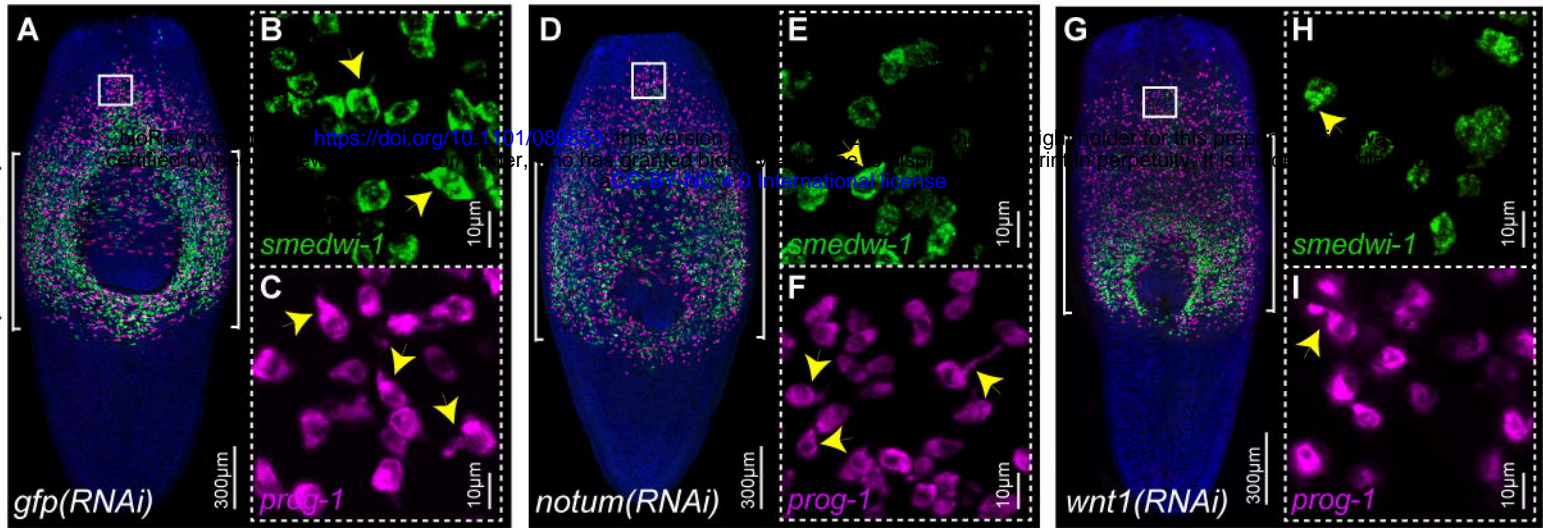




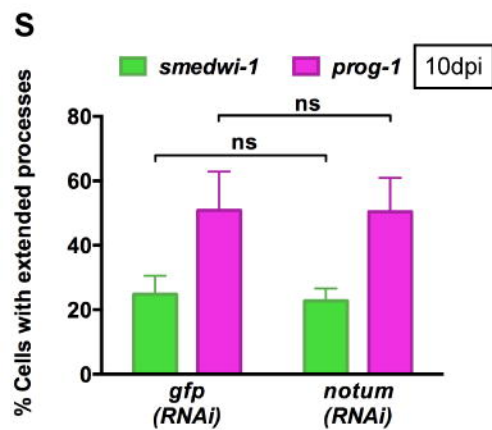
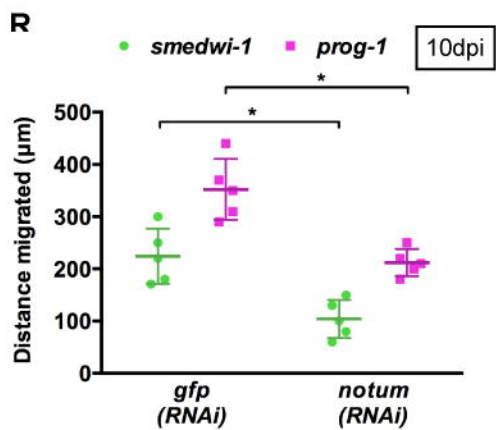
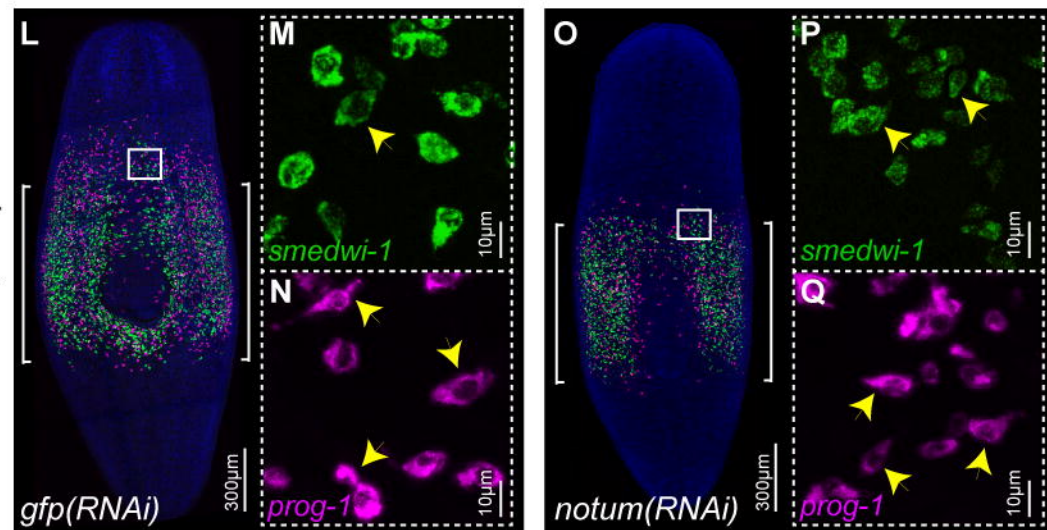
**L** Model of anterior signal



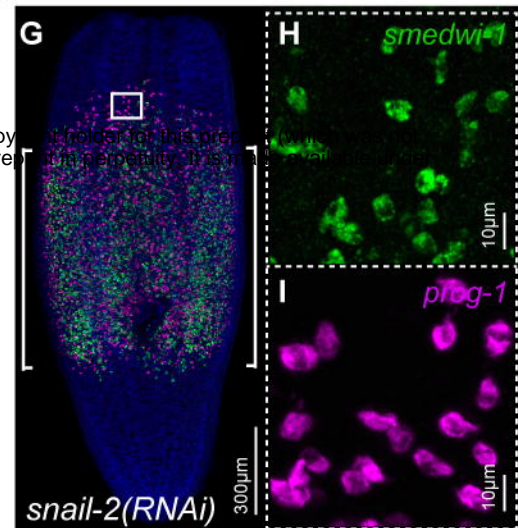
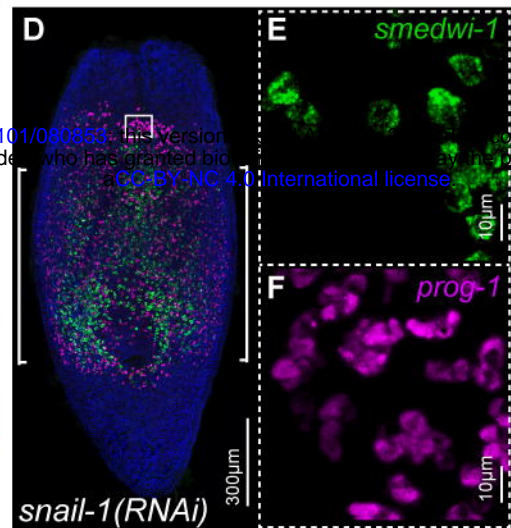
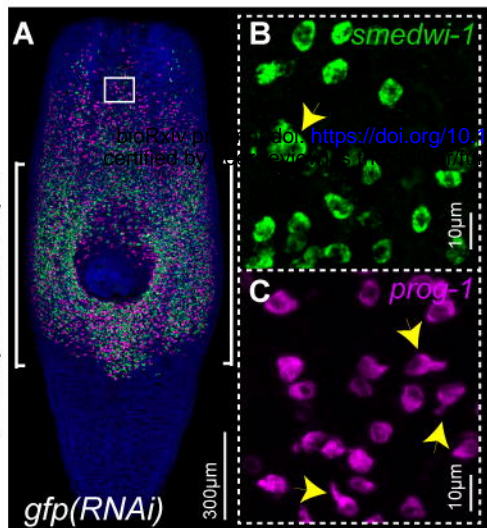
Decapitated, 7dpa



Intact, 10dpi



Decapitated, 7dpa



Decapitated, 7dpa

